Processes in Optical Diesel Engines - Emissions Formation and Heat Release

Aronsson, Ulf

2011

Processes in Optical Diesel Engines

-Emissions Formation and Heat Release

Ulf Aronsson

Doctoral Thesis

Division of Combustion Engines
Department of Energy Sciences
Faculty of Engineering
Lund University

LUND UNIVERSITY

ISBN: 978-91-7473-116-3
ISRN LUTMDN/TMHP-11/1080 – SE
ISSN 0282-1990

Division of Combustion Engines
Department Energy Sciences
Faculty of Engineering
Lund University
P.O. Box 118
SE-22100 Lund
Sweden

Printed in Sweden by Tryckeriet i E-huset, Lund March 2011

List of publications

Paper I

Heat Release Comparison Between Optical and All-Metal HSDI Diesel Engines
Ulf Aronsson, Clément Chartier, Uwe Horn, Öivind Andersson, Bengt Johansson, Rolf Egnell

Division of Combustion Engines, Lund University, Sweden

SAE Technical paper 2008-01-1062

Paper II

Analysis of the Correlation Between Engine-Out Particulates and Local Φ in the Lift-Off Region of a Heavy Duty Diesel Engine Using Raman Spectroscopy
Ulf Aronsson[1], Clément Chartier[1], Öivind Andersson[1], Rolf Egnell[1]
Johan Sjöholm[2], Mattias Richter[2], Marcus Aldén[2]

[1]Division of Combustion Engines, Lund University, Sweden
[2]Division of Combustion Physics, Lund University, Sweden

SAE Int. J. Fuels Lubr. October 2009 2:645-660/2009-01-1357

Paper III

Influence of Spray-Target and Squish Height on Sources of CO and UHC in a HSDI diesel engine during PPCI Low-Temperature Combustion
Ulf Aronsson[1], Öivind Andersson[1], Rolf Egnell[1]
Paul C. Miles[2,1], Isaac W. Ekoto[2]

[1]Division of Combustion Engines, Lund University, Sweden
[2]Sandia National Laboratories, Livermore, CA, United States

SAE Technical paper 2009-01-2810

Paper IV

Analysis of EGR Effects on the Soot Distribution in a Heavy Duty Diesel Engine using Time-Resolved Laser Induced Incandescence

Ulf Aronsson[1], Clément Chartier[1], Öivind Andersson[1], Bengt Johansson[1]
Johan Sjöholm[2], Rikard Wellander[2], Mattias Richter[2], Marcus Aldén[2]
Paul C. Miles[3,1]

[1]Division of Combustion Engines, Lund University, Sweden
[2]Division of Combustion Physics, Lund University, Sweden
[3]Sandia National Laboratories, Livermore, CA, United States

SAE Int. J. Engines December 2010 3:137-155 /2010-01-2104

Paper V

Impact of Mechanical Deformation due to Pressure, Mass, and Thermal Forces on the In-Cylinder Volume Trace In Optical Engines of Bowditch Design

Ulf Aronsson, Hadeel Solaka, Clément Chartier, Öivind Andersson, Bengt Johansson

Division of Combustion Engines, Lund University, Sweden

SIAT paper number 119 /SAE Technical paper 2011-26-008

Paper VI

Analysis of Errors in Heat Release Calculations due to Distortion of the In-Cylinder Volume Trace from Mechanical Deformation for Optical Diesel Engines

Ulf Aronsson, Hadeel Solaka, Guillaume Lequien, Öivind Andersson, Bengt Johansson

[1]*Division of Combustion Engines, Lund University, Sweden*

Submitted to International Journal of Engine Research

Paper VII

UHC and CO Emissions Sources from a Light-Duty Diesel Engine Undergoing Dilution Controlled Low-Temperature Combustion

Isaac W. Ekoto[1], Will F. Colban[1], Paul C. Miles[1,3]
Sung Wook Park[2], David E. Foster[2], Rolf D. Reitz[2]
Ulf Aronsson[3], Öivind Andersson[3]

[1]*Sandia National Laboratories*
[2]*University of Wisconsin Engine Research Center*
[3]*Division of Combustion Engines, Lund University, Sweden*

SAE Int. J. Engines March 2010 2:411-430/2009-24-0043

Paper VIII

UHC and CO Emissions Sources from a Light-Duty Diesel Engine Undergoing Late-Injection Low Temperature Combustion

Isaac W. Ekoto[1], Will F. Colban[1], Paul C. Miles[1,2]
Ulf Aronsson[2], Öivind Andersson[2]
Sung Wook Park[3], David E. Foster[3], Rolf D. Reitz[3]

[1]*Sandia National Laboratories*
[2]*Division of Combustion Engines, Lund University, Sweden*
[3]*University of Wisconsin Engine Research Center*

Proceedings of the ASME Internal Combustion Engine Division Fall Technical Conference ICEF September 27-30, 2009, Lucerne, Switzerland

Other related publications

Analysis of Smokeless Spray Combustion in a Heavy-Duty Diesel Engine by Combined Simultaneous Optical Diagnostics

Clément Chartier[1], Ulf Aronsson[1], Öivind Andersson[1], Rolf Egnell[1]
Robert Collin[2], Hans Seyfried[2], Mattias ,Richter[2], Marcus Aldén[2]

[1]*Division of Combustion Engines, Lund University*
[2]*Division of Combustion Physics, Lund University*

SAE Technical paper 2009-01-1353

Challenges for In-cylinder High-Speed Two-Dimensional Laser-Induced Incandescence Measurements of Soot
Johan Sjöholm[1], Rikard Wellander[1], Mattias Richter[1], Marcus Aldén[1]
Ulf Aronsson[2], Clément Chartier[2], Öivind Andersson[2], Bengt Johansson[2]

[1]Division of Combustion Physics, Lund University, Sweden
[2]Division of Combustion Engines, Lund University, Sweden

SAE Technical paper 2011-01-1280

Influence of Jet-Jet Interactions on the Lift-Off Length in an Optical Heavy-Duty DI Diesel
Clément Chartier, Ulf Aronsson, Öivind Andersson, Rolf Egnell, Bengt Johansson

Division of Combustion Engines, Lund University, Sweden

Submitted to International Journal of Engine Research

Effect of Injection Strategy on Cold Start Performance in an Optical Light-Duty DI Diesel Engine
Clément Chartier, Ulf Aronsson, Öivind Andersson, Rolf Egnell

Division of Combustion Engines, Lund University, Sweden

SAE Int. J. Engines March 2010 2:431-442/2009-24-0045

Abstract

This project deals with questions related to generic diesel combustion research and optically accessible engines are used to study the combustion process. Images of the combustion are analyzed together with in-cylinder pressure and exhaust gas emission measurements. The results can be divided into two main categories: one about evaluations of optically accessible engines and one about studies of emissions and heat release. The focus is on the link between the combustion event and engine-out emissions. The reason for putting efforts on the first category is to get more reliable information from the second one.

First, the mechanical behaviour during operation of optical engines is discussed. Optical engines may suffer from distortion of the in-cylinder volume trace due to mechanical deformation from mass, pressure and thermal forces. This distortion causes errors in heat release calculations. A method to account for the errors is therefore developed which makes the calculations insensitive to mechanical deformations.

The optical access also affects the engines heat transfer properties which can cause differences in heat release and engine-out emissions compared to all-metal engines. Fortunately, it is possible to compensate for the differences and achieve realistic engine-out emissions and combustion phasing by adjusting the charge temperature.

The engine-out soot emissions are the result of a complex series of events including fuel air mixing, premixed combustion, mixing controlled combustion, and late soot oxidation. The first part of the emission section in this thesis deals with factors that are known to be important for the soot formation and estimates how they affect the engine-out soot emissions. The goal is to identify characteristics of the soot formation that are important for the engine-out smoke level and thereby the soot particle mass. Two studies are included in this chapter, one about air entrainment and one about early soot formation. It is indicated that the rate of soot-formation during the quasi-steady jet-phase has a rather weak relation to the level of engine-out soot. This is despite the usage of few, small, nozzle holes leading to a long injection duration with a large portion of the combustion taking place during the fuel injection period. The observation is explained as follows: First, a large fraction of the soot is formed in the transition between the premixed and spray-driven combustion which weighs down the importance of the quasi-steady jet-phase. Second, factors that enhance the soot formation during the jet phase in some cases also enhances the soot oxidation during this phase. Third, correlations to emissions of CO and UHC further point to the importance of the oxidation process and characteristics of the heat release indicates that this is partly related to the late cycle.

The second part of the emission section deals with the sources of CO and UHC during low temperature combustion. It is suggested that the squish volume is crucial for the engine-out CO and UHC levels during low load. Two combustion concepts with different injection strategies are investigated, one with very early start of injection (SOI) and one with SOI close to TDC. The squish volume is indicated to be the major source of not fully oxidized products in both cases which shows that the importance of this source is not easily erased.

Acknowledgements

Many people have contributed to the content of this thesis and I am grateful to all of them.

I would like to start by thanking my main supervisor Öivind Andersson. Öivind is a good friend and mentor and is always willing to expend great efforts in helping his students.

Paul Miles at Sandia National laboratories functioned as my supervisor for parts of the project, he has always been a pleasure to work with and really fun to hang out with. Paul's deep knowledge certainly improved the work presented in this thesis.

I want to thank my assistant supervisors Bengt Johansson and Rolf Egnell for being helpful and supportive during the whole PhD project. Mattias Richter at the combustion physics division has been a great support during the extensive laser measurement campaigns.

During my laboratory work I have always felt well supported by technicians. Jan Erik Nilsson kept the lab in perfect shape during the first years and when he retired Kjell Jonholm continued in the same manner. Krister Olsson has always been helpful in supplying computer programs.

Our reference group from the industry, the Gendies group, has been inspiring to work with and a source of ideas for new experiments. Special thanks goes to Jan Eismark, Johan Forss, Joop Somhorst, and Håkan Persson.

I would also like to thank all my friends and colleagues at the division of combustion engines, it has been fun to work with all of them. Special thanks goes to Clément Chartier, Hadeel Solaka, and Guillaume Lequien for being good friends and for having contributed to the work presented in this thesis. I also want to thank Martin Algotsson for help with the proof reading. Finally, I'd like to thank Magnus Lewander, Ida Truedsson, Peter Andersson, Teemu Anttinen, Hans Aulin, Claes-Göran Zander, and Mengqin Shen for being supportive and fun to hang out with.

Nomenclature

ATDC	-After Top Dead Center
BDC	-Bottom Dead Center
C_2	-C_2 Radical
CA50	-Crank Angle degree at 50% heat release completion
CAD	-Crank Angle Degree
CI	-Compression Ignition
CLD	-ChemiLuminescence Detection
CO	-Carbon monoxide
DI	-Direct Injected
EGR	-Exhaust Gas Recirculation
EOI	-End Of Injection
FID	-Flame Ionization Detector
FSN	-Filtered Smoke Number
GUI	-Graphical User Interface
ID	-Ignition Delay
IMEP	-Indicated Mean Effective Pressure
$IMEP_g$	-Gross Indicated Mean Effective Pressure
IR	-InfraRed
IVC	-Inlet Valve Closing
LII	-Laser Induced Incandescence
LIF	-Laser Induced Fluorescence
LIFF	-Laser Induced Fragmentation Fluorescence
LTC	-Low Temperature Combustion
MK	-Modulated Kinetics
NDIR	-Non-Dispersive InfraRed
NO_x	-Nitrogen Oxides
O_3	-Ozone
OH	-Hydroxyl radical
PAH	-PolyAromatic Hydrocarbons
PHR	-Premixed Heat Release
PCI	-Premixed Compression Ignition
PIV	-Particle Image Velocimetry
PLIF	-Planar Laser Induced Fluorescence
PM	-Particulate Matter
PPC	-Partially Premixed Combustion
PPCI	-Partially Premixed Compression Ignition
SCR	-Selective Catalytic Reduction
SOI	-Start Of Injection
TDC	-Top Dead Center
UHC	-Unburned HydroCarbons
UNIBUS	-UNIform BUlky combustion System
UV	-UltraViolet

Table of Content

Chapter 1

Introduction

1.1 Background

The diesel engine, named after its inventor Rudolf Diesel, was patented in 1892 and has since substantially contributed to our societies development [1]. The diesel engines most important use is as a power source in vehicles and the importance still increasing. The share among new registered passenger cars in western Europe has increased from 14% in 1990 to about 50% in 2010 [2]. For commercial vehicles, both on land and at sea, it has been the most important power source for decades.

Despite its long history, the demand for improvements of the diesel engine are still high. In the beginning the focus was on performance and durability, nowadays pollutant legislations and demand for higher efficiency force continuous redesigns. The focus is to develop fuel efficient diesel engines with minimum environmental impact.

The legislated emissions from diesel engines are: Particulate Matter (PM), nitrogen oxides (NO_x), Unburned HydroCarbons (UHC), and carbon monoxide (CO). A fifth emission that is not legislated, so far, but in some countries encouraged to be decreased with tax incentives is carbon dioxide (CO_2). The four legislated emissions are largely affected by the characteristics of the combustion process while the CO_2 emissions are proportional to the fuel consumption.

The engine manufacturers have strict demands from two directions: the legislated emission levels have to be reached while the consumers require low cost and high performance. There are different possible paths to reach these demands and the key is to meet the regulatory requirements with as high performance and low cost as possible.

Lately different hybrid concepts have frequently been proposed where a diesel engine works together with an energy storage device such as a battery or a pressure tank [3,4]. The usage of such concepts improves the overall fuel economy and specific engine-out emissions significantly. Simultaneously, the aftertreatment systems for diesel engines have become more efficient. Diesel engines can be equipped with particulate filters that decrease the amount of particulates, and

NO_x can be handled by Selective Catalytic Reduction (SCR) systems or NO_x traps. CO and UHC can be reduced with oxidation catalysts. However, hybridisation and aftertreatment systems increase the cost of the drive line significantly. Furthermore, NO_x traps and particulate filters impair the efficiency of the engine and SCR requires that a reduction agent is continuously added (ammonia or urea). It is thereby desirable to reduce the emissions already inside the cylinder. To reach future emission legislation limits it is likely that every part of the vehicle has to be optimized, meaning that hybridization and aftertreatment are used in combination with advanced combustion concepts.

1.2 Objective

The goal with this work is to answer diesel combustion related questions. The focus is on the coupling between combustion events and engine-out emissions. The experimental work is performed on optical engines which are essentially engines with parts of the combustion chamber replaced with transparent materials. Much effort is also spent on evaluation of how the modifications to get optical access affect the combustions phasing and dynamic behaviour of the engine. This is to investigate the suitability of optical engines as models of all-metal engines and also to learn how to operate and interpret data from these engines. The work is performed in close collaboration with the industry and the questions reflect some of the problems the diesel engine manufacturers will be facing in the future.

1.3 Method

The approach in this thesis is optical investigations of diesel combustion. The usage of optical engines gives the opportunity to study the combustion process in detail. The combustion can be studied passively with a camera or actively, where specific emissions are accentuated with assistance of lasers. Besides the optical investigations, engine-out emission and pressure measurements are performed. The in-cylinder pressure trace contains information about both the load and the phasing of the combustion. The combustion phasing is closely related to the formation of emissions inside the engine.

1.4 Thesis contributions

This thesis presents novel insights about 1) how to operate optical engines in order to get realistic combustion phasing and engine-out emissions, 2) how to consider dynamic aspects of different engine components in order to make a more accurate pressure analysis, 3) the relation between characteristics of soot formation and the engine-out soot emissions, and finally 4) the sources of CO and UHC during low temperature combustion. These contributions will be discussed in detail in chapter 4 and 5.

Chapter 2

Diesel engine diagnostics

2.1 Optical engines

The objective of optical engines is to gain visual access to the combustion chamber by manufacturing parts of the wall in transparent material. Different materials are used but sapphire and quartz are the most common. To simplify the terminology glass is used as a generic term here. Normally when multi-cylinder engines are rebuilt to get optical access they are only operated on one cylinder. The amount of optical access varies. Some optical engines only have access through an endoscope and others have most of the combustion chamber manufactured in glass. Figure 1 illustrates an optical engine of Bowditch design. It has optical access to the combustion chamber from the side through the cylinder liner and from below through the piston crown. To make this possible the cylinder head is lifted up, the piston is extended, and an angled mirror is placed in the bottom of the hollow piston extension. Since the combustion can be studied both from the side and from below this design is suited for laser diagnostics where the imaging normally is performed perpendicular to the laser beam. The beam is sent in through the liner and radiation is imaged through the piston crown via the mirror or through the liner perpendicular to the beam.

Since all diagnostics of optical engines are performed to understand the combustion process in all-metal engines it is desirable to make as small changes of the engine as possible. The combustion process might be affected by changes in heat transfer and flow pattern. The optical access impairs the heat transfer in the engine for two reasons: Glass is a much poorer heat conductor than steel and aluminium and it is not possible to have water cooling of the glass parts. It is also common to move the piston rings in order to avoid them passing the joint between glass and steel in the liner. This affects the in-cylinder flow pattern and the compression ratio. Nevertheless optical engines are useful tools to investigate diesel combustion and the changes introduced are possible to compensate for [5,6]. This topic is further discussed in chapter 4.

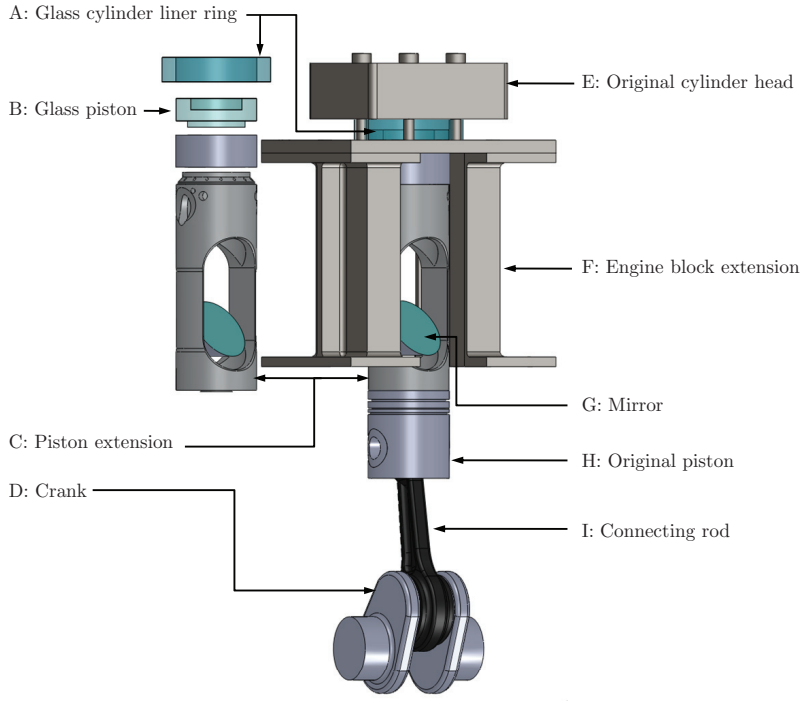

Figure 1 - Optical engine of Bowditch design. Items A, B, C, F, and G are added to achieve optical access to the combustion chamber while the rest are all-metal engine parts.

In this project, combustion in both light- and heavy-duty diesel engines of Bowditch design are studied. The heavy-duty engine is a Scania engine with a displacement of 1.95 l per cylinder. Two light-duty engines are studied; one Volvo engine and one GM engine. Both have a displacement of 0.48 l per cylinder. Finally, a light-duty all-metal Volvo engine is studied to compare with the optical data. All engines are operated on one cylinder. See Table 1.

The engine lab housing engine 1 and 2 is equipped with a system for simulating Exhaust Gas Recirculation (EGR), consisting of an external diesel furnace for domestic heating. The EGR can be mixed with the inlet air and conditioned using a mechanical compressor and an electric heater. This allows independent

Table 1 - Engines used in experiments.

Engine	1	2	3	4
Displacement vol. [l]	1.95	0.48	0.48	0.48
Bore [mm]	127	81	82	81
Stroke [mm]	154	93.2	90.4	93.2
Optical [Y/N]	Y	Y	Y	N
Manufacturer	Scania	Volvo	GM	Volvo

control of inlet O_2 mole fraction, boost pressure and temperature. Engine 3 is instead fed by a mixture of air, nitrogen, and CO_2 in desired proportions. The inlet temperature is controlled by an electric heater and the total gas flow regulates the inlet pressure. Engine 4 use its original EGR systems but the inlet pressure and temperature can be adjusted externally.

2.2 Optical diagnostics

Depending on the purpose of the optical engine investigation, different diagnostic techniques are used. There are two main classifications of optical measurement techniques; passive and active. In passive techniques the combustion is imaged as it is without interference. All passive optical measurement techniques give a line-of-sight perspective of the combustion chamber. Therefore it is impossible to image the inside of a reacting diesel flame with passive measuring techniques. Another limitation is that only species that radiate naturally can be imaged. In active optical measurement techniques however, an external radiation source is used to actively generate the radiation from the measurement volume. This gives the opportunity to investigate the interior of the flame and more species can be studied. Active optical measurement techniques can be used to measure in a point, along a line, in a plane, or in three dimensions. The three dimensional measurements consist of several spatially dispersed planar images captured over a short time period. In combustion engine diagnostics the dominant radiation source is lasers and other radiation sources are not considered here. [7,8]

Passive optical diagnostics

The most basic technique is to image the combustion with a camera. This shows the natural combustion radiation i.e. of soot luminosity and chemiluminescence from different gas molecules. The soot luminosity is normally dominant and emits radiation over the whole spectrum as a black body radiator. The chemiluminescence arises from excited combustion radicals. When certain radicals are studied the camera can be equipped with a band-pass spectral filter that separates the studied wavelength.

One commonly imaged species is the hydroxyl radical (OH). This is an important intermediate species in high temperature chemistry [8]. Images of OH thereby give information of where high temperature reactions occur. The detection apparatus must be UltraViolet (UV) sensitive since the OH radical emit light near 308 nm which is in the UV wavelength domain.

Lasers

In active optical measurement techniques it is common to use a laser source. A laser consists of a cavity and an active medium. The cavity is a volume with mirrors at two sides facing each other. Inside the cavity the active medium is placed which can be a solid, a liquid, or a gas. Energy is added to the active

medium in order to excite the molecules into a higher energy level. This process is called pumping. The energy is usually in form of light or an electric discharge. The molecules can relax to their ground state in two ways; spontaneously, or stimulated by photons with the same energy as the transition between the energy levels. When the relaxation is spontaneous photons may be emitted in any direction while stimulated emission has the same direction and phase as the triggering photon.

The active medium acts as an amplifier if it has inverse populations i.e. if more molecules are in the higher than in the lower energy level. It is not feasible to obtain inverse population in a two level system and hence three or four level systems, as illustrated in Fig. 2, are used. Three level systems rely on a very fast radiationless transition from the third to the second level. The lasing transition is between the second and first level as can be seen in Fig. 2. The upper level in the lasing transition has a long lifetime, which is the prerequisite for obtaining an inverse population. Four level lasers has its lasing transition between the third and second level while the other transitions are fast and radiationless. Since second level has a short lifetime it is possible to achieve inverse population even with quite low population in the third level. The word Laser is the abbreviation of Light Amplification by Stimulated Emission of Radiation. [8,9]

In summary, the working principle of a laser is as follows: the active medium is pumped with energy until inverse population is obtained. Photons are emitted spontaneously. A fraction of these photons starts to oscillate between the facing mirrors and passes through the active medium during each round trip. Since the photons have the same energy as the active transition new photons are emitted by stimulated emission. The active medium acts as an amplifier, thus the number

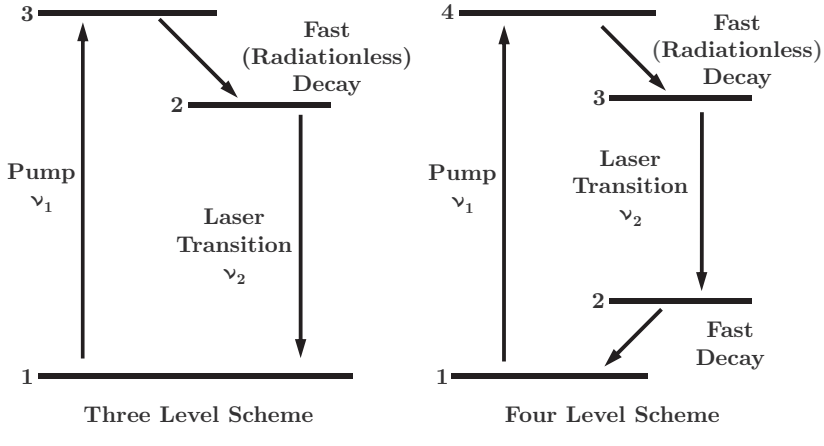

Figure 2 - Energy levels for three and four level lasers, adopted from [10].

of oscillating photons increase each round trip. One of the mirrors is semi-transparent in order to let some of the radiation escape as the laser beam. [8,9]

Lasers used in combustion diagnostics are normally pulsed. Pulsed lasers rely on a switch that can very fast change the quality factor, or Q-factor, of the oscillator. This is called a Q-switch. When the Q-factor is high the losses each round trip is low compared to the stored energy and vice versa. A closed Q-switch prevents the photons from oscillating inside the cavity which minimizes the stimulated emissions. This allows a larger number of electrons to gather in the higher energy level. When the Q-switch opens, and let the photons through, a short high power laser pulse is created that is utilized for combustion diagnostics. [8,9]

Elastic scattering

In elastic scattering any laser wavelength can be used and the detected light has the same wavelength as the laser. The laser light that is sent into the engine is scattered from different molecules and particles but the photons keep their energy and thereby their wavelength. Elastic scattering is easy to achieve and the technique is suited for planar imaging.

Depending on the size of the scattering objects the behaviour is different. For molecules or particles that are much smaller than the laser wavelength the denotation is Rayleigh scattering. The signal strength, I, of Rayleigh scattering shows a very strong dependence on the wavelength, λ,

$$I \propto \frac{1}{\lambda^4} \tag{1}$$

A shorter wavelength thereby gives a stronger signal. In combustion diagnostics, Rayleigh scattering can be used to image zones that contain vapour-phase fuel. Rayleigh scattering is polarization dependent which means that the laser polarization needs to be considered.

When the light is scattered from particles that have a size that is comparable to or larger than the laser wavelength it is called Mie scattering. Contrary to Rayleigh scattering, Mie scattering does not show a strong wavelength dependence. In combustion engine diagnostics, Mie scattering can be used to image liquid fuel droplets and soot particles. If there are larger particles in the measurement volume the Mie signal will strongly dominate the Rayleigh signal. Accordingly, if fuel vapor is to be imaged with Rayleigh scattering it is crucial to avoid illumination of liquid fuel droplets. [8]

Raman scattering

In Raman scattering molecules are excited to a virtual level. The scattered radiation from when they fall back to their ground state is inelastic, meaning that

the radiation has another wavelength than the laser. The change in wavelength is given by the Raman shift for a given species. The Raman shift is molecule-specific which gives the ability to measure the concentrations of all major species simultaneously. The signal is normally detected on a spectrometer where spectral peaks appear at a distance from the laser wavelength that is given by the Raman shift. The only requirements for detecting multiple species with Raman scattering are that the signals from the different molecules have sufficient intensity and do not overlap too much spectrally. The Raman scattering is very weak and elastic scatter at the laser wavelength might have to be filtered out so that the spectrum will not be saturated. Since the signal needs to be analyzed spectrally, planar Raman spectroscopy requires advanced detection systems. [8]

Laser-induced fluorescence

Laser Induced Fluorescence (LIF) is the optical radiation from laser excited molecules that return from a higher to a lower energy state. The LIF signal strength depends on the cross section of the studied molecule. Different molecules are absorbing (have a large cross section) at different laser wavelengths. The choice of wavelength is thereby linked to the studied molecule. An excitation scan, where the laser is tuned to the wavelength where the signal is maximized, can precede the experiments. The fluorescence is usually detected at a longer wavelength than the laser and can be imaged with a camera or spectrally resolved. LIF provides high signal strength and also minor species can be imaged. If the detection is two-dimensional the denotation is Planar Laser Induced Fluorescence (PLIF). [8]

Laser-induced incandescence

Laser Induced Incandescence (LII) is created by a laser pulse heating soot particles to a temperature significantly higher than the surrounding medium. Since the laser heated soot particles are much hotter than the surrounding gas their emitted light-spectra are blue shifted compared to the surrounding cooler particles. The blue shifted LII signal is usually collected at short wavelengths where the flame background luminosity is insignificant. LII can be utilized to measure both soot volume fraction and soot particle size. The decay time of the LII signal is related to the soot particle size and the signal strength is related to the soot volume fraction. [8]

2.3 Heat release

If the pressure inside the cylinder as function of volume is known, the apparent heat release can be calculated. The in-cylinder volume as function of crank angle, ϑ, can be expressed as [11],

$$V = V_c + \frac{V_d}{2}\left(R + 1 - cos\,\vartheta - R\left(1 - \left(\frac{sin\,\vartheta}{R} - \frac{\Psi}{l} \right)^2 \right)^{0.5} \right) \tag{2}$$

where V_d is the displacement volume, V_c the compression volume, R is the ratio between the connecting rod and the crank radius, Ψ is the piston pin offset, and l is the length of the connecting rod. The apparent heat release gives information about the combustion process and is a useful tool in combustion engine diagnostics. The following is a description of the heat release theory in [12,13]. In heat release analysis the cylinder is considered a thermodynamic system with uniform pressure and temperature. According to the first law of thermodynamics the energy balance of such a system can be expressed as

$$\frac{dQ}{dt} = \frac{dU}{dt} + \frac{dW}{dt} + \sum_i m_i h_i \tag{3}$$

where dQ/dt is the heat added to the system, dU/dt is the change in internal energy, dW/dt is the work performed by the system, m is the mass, and h is the enthalpy for an element, i, that enters the system. The internal energy, U, can be expressed as

$$U = mC_v T \tag{4}$$

where C_v is the specific heat at constant volume and T is the temperature. If the mass in the system is constant the derivative of U is

$$\frac{dU}{dt} = mC_v \frac{dT}{dt} \tag{5}$$

From the ideal gas law

$$pV = mRT \tag{6}$$

where V is the volume and R is the specific gas constant, it follows that

$$\frac{dT}{T} = \frac{dV}{V} + \frac{dp}{p} \tag{7}$$

if R and m are taken to be constant. Using Eq. 6 and 7, Eq. 5 can be rewritten in the form

$$\frac{dU}{dt} = \frac{C_v}{R}\left(p\frac{dV}{dt} + V\frac{dp}{dt} \right) \tag{8}$$

The work performed by the system can be expressed as

$$\frac{dW}{dt} = p\frac{dV}{dt} \tag{9}$$

Neglecting mass exchange and using Eq. 8 and 9, Eq. 3 can be rewritten as

$$\frac{dQ}{dt} = \frac{C_v}{R}\left(p\frac{dV}{dt} + V\frac{dp}{dt}\right) + p\frac{dV}{dt} \tag{10}$$

The specific gas constant can be expressed as

$$R = C_p - C_v \tag{11}$$

where C_p is the specific heat ratio at constant pressure. Eq. 11 and the ratio

$$\gamma = \frac{C_p}{C_v} \tag{12}$$

can be used to simplify Eq. 10 into

$$\frac{dQ}{dt} = \frac{\gamma}{\gamma - 1}p\frac{dV}{dt} + \frac{1}{\gamma - 1}V\frac{dp}{dt} \tag{13}$$

Since both the volume and pressure trace are more commonly expressed as a function of Crank Angle Degree (CAD), ϑ, Eq. 13 is more useful in the form

$$\frac{dQ}{d\vartheta} = \frac{\gamma}{\gamma - 1}p\frac{dV}{d\vartheta} + \frac{1}{\gamma - 1}V\frac{dp}{d\vartheta} \tag{14}$$

which is referred to as the apparent heat release. The above procedure assumes zero mass transport across the system boundary. In reality this is not the case. To handle the mass losses mathematically correct requires Eq 5 to be rewritten which affects the subsequent steps. It is, however, more common to assume that the mass losses are small enough to be handled in a separate term

$$\frac{dQ}{d\vartheta} = \frac{\gamma}{\gamma - 1}p\frac{dV}{d\vartheta} + \frac{1}{\gamma - 1}V\frac{dp}{d\vartheta} + \frac{dQ_{losses}}{d\vartheta} \tag{15}$$

where dQ_{losses} consists of mass losses combined with heat losses. The losses decrease the in-cylinder pressure and if they are not considered, the calculated

heat release is lower than the actual heat release. The mass losses mainly consist of leakage over the piston rings. This is called blow by.

There are different approaches to handle heat and mass-losses. Both physical and mathematical methods are described in the literature [12-15]. The mathematical methods do not distinguish between heat and mass losses. The idea is to use known facts about the heat release and adjust parameters to get a reasonable shape of the heat release. For example, before start of injection the rate of heat release should be zero. The physical methods quantify the losses according to the specifications of the engine and the in-cylinder conditions.

The mass losses can be estimated as a compressible flow through a nozzle. The speed of compressible flows through nozzles does not depend on the pressure drop over the nozzle if the pressure ratio is high enough [16,17]. This is because the flow gets choked and reaches a maximum speed close to the speed of sound. However, the mass flow

$$\dot{m} = A \cdot p_0 \sqrt{\frac{\gamma}{RT_0}} \left(\frac{2}{\gamma+1} \right)^{(\gamma+1)/(2(\gamma-1))} \tag{16}$$

does not get choked since it apart from the nozzle cross section area, A, depends on the stagnation properties p_0 and T_0 of the flow [17]. In [12] it is experimentally verified that the blow by has a linear dependence on the smallest piston ring gap. The mass losses can thereby be estimated by Eq. 16 with the piston ring gap as A and the in-cylinder pressure p_0. The temperature in the top-land volume will depend on both in-cylinder mean temperature and wall temperature.

The convective heat transfer, dQ_{HT}/dt, to the cylinder wall depends on the heat transfer coefficient, h, the wall area, A_{wall}, and the difference between the mean gas-temperature and the mean wall temperature [12]:

$$\frac{dQ_{HT}}{dt} = h \cdot A_{wall} \left(T_{gas} - T_{wall} \right) \tag{17}$$

Woschni has developed the following relation for the heat transfer coefficient [14],

$$h = 3.26 \cdot B^{-0.2} \cdot p^{0.8} \cdot T^{-0.55} \cdot w^{0.8} \tag{18}$$

where B is the cylinder bore and w is a characteristic speed that follows the relation;

$$w = C_1 S_p + C_2 \left(\frac{V_d \cdot T_{ivc}}{p_{ivc} \cdot V_{ivc}} \right) \left(p_c - p_m \right) \tag{19}$$

where S_p is the mean piston speed, V_d is the swept volume, V_{ivc}, is the volume at Inlet Valve Closing (IVC), p_c is the pressure during the fired cycle, p_m the pressure during a motored cycle, p_{ivc} is pressure at IVC, T_{ivc} is the temperature at IVC, C_1 and C_2 are parameters to adjust the heat transfer to a specific engine. The pressure in Eq. 18 should be in kPa.

A useful and simpler method to improve the heat release calculations is to subtract the heat release from a motored cycle from the fired heat release [18]. This compensates partly for the heat-losses, mass losses, and errors in the calculated volume.

There are many challenges in heat release calculations. First, the piezo electric pressure transducer does not give the absolute pressure; it only gives information about the pressure change between two consecutive measurements. Therefore the pressure trace has to be locked to a known, absolute pressure in one position to make the information useful. Second, γ varies with gas composition and temperature [19]. Third, it is not as trivial as it might seem to obtain an exact volume trace. Mechanical deformation from thermal, gas and mass forces has an impact on the engine geometry which causes a distorted volume trace. This topic is discussed in detail in chapter 4. Last, the losses from the system are hard to estimate. Heat release analysis should therefore be considered as an approximation rather than an exact method.

In this project a heat release program was developed to be used in the analysis. The program is developed in Java and uses the theory described above. Java is a powerful, object oriented programming language [20,21]. One of the strongest qualities with Java is that it is platform independent [20]. The program reads pressure traces from files and it calculates the volume as a function of CAD. The pressure and volume are then used to calculate the heat release. The program gives the ability to choose between mathematical and analytical heat- and mass-loss management.

The pressure trace can be locked to the inlet pressure, a given polytropic coefficient, or mathematically to the pressure level that gives a constant polytropic constant during a part of the compression, as described in [15]. The program has two different models for the temperature dependence of γ, a linear dependence described in [12] and an exponential dependence described in [19]. The Graphical User Interface (GUI) is developed with the java Swing package, see Fig. 3.

From the GUI geometrical data of the engine, information about the operating condition and parameters used in the calculation can be specified. When the calculations are performed, all data are saved in a separate folder and are reloaded automatically the next time the pressure trace is to be analyzed. The

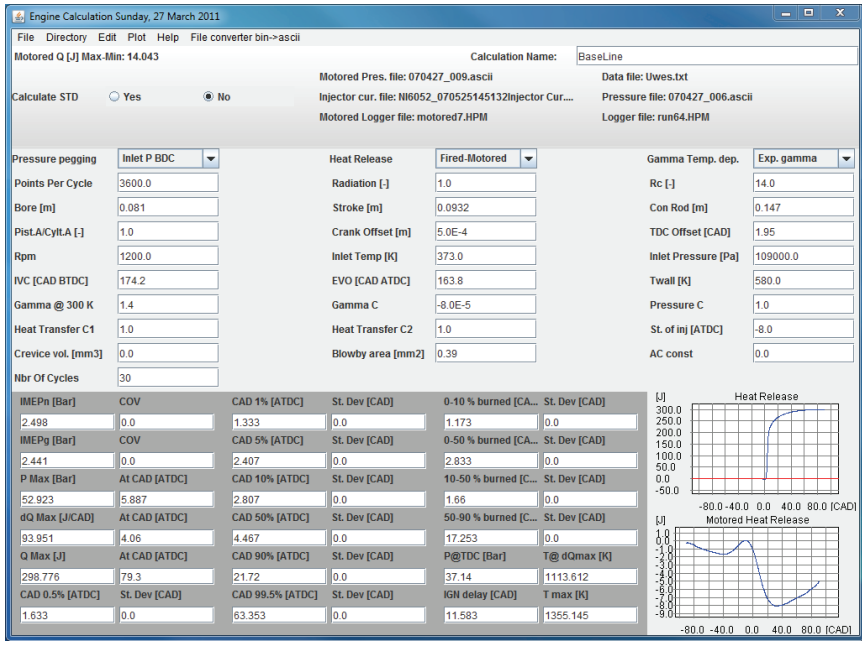

Figure 3 - GUI from heat release program.

result in terms of combustion phasing, load and ignition delay are displayed in the dark gray area of the GUI in Fig. 3. The pressure, rate of heat release, cumulative heat release, temperature, and heat transfer can be plotted from the GUI in a self-developed plot function. All results are also stored in files so they can be reached outside of the program.

2.4 Emission measurements

One prioritized field in combustion engine research is to minimize pollutants and therefore emission measurements are essential. While optical diagnostics and heat release analysis are performed to analyze the combustion process, emission measurements give information about how eligible the operating condition is. The most important harmful pollutants from diesel engines are PM, NO_x, UHC, and CO. PM consists of solid and liquid particles. A significant contribution to PM comes from combustion-generated soot particles. The EU emission standards can be found in Table 2 and 3. Table 2 shows the standards for heavy duty diesel engines and Table 3 shows the standards for diesel engine passenger cars. The levels in Table 2 are expressed in g/kWh while the levels in Table 3 have the unit g/km. The standards thereby relate emissions directly to engine performance for heavy-duty engine and to the whole vehicle for passenger cars. In [13] the energy needed for a passenger car driving on a highway is estimated to 0.14 kWh/km, an

approximate comparison between the levels in Tables 2 and 3 can be made by dividing the numbers in Table 3 with this factor.

In addition to the particle mass limit, a particle number limit is going to be effective for both passenger cars and heavy duty vehicles. The number limit would prevent the possibility that the particle mass limit is met using "open filters" that allows a high number of ultra fine particles to pass. The emission standards become more stringent with every step which forces continuously changing combustion strategies. The different tiers in Table 2 are related to different test cycles and therefore the levels cannot be directly compared. [22]

Smoke

The measurement procedure of PM is complex. Therefore it is more common with smoke value measurements during engine tests [23]. Smoke can be measured as a Filtered Smoke Number (FSN) where a given volume of exhausts is drawn through a white paper filter. The black smoke particles are trapped on the filter and the darkness of the filter determines the FSN value. The darkness is evaluated from the reflection from the filter paper. Zero reflection is equal to a filtered smoke number of 10 and a clean filter is equal to 0 FSN. Empirical

Table 2 - EU emission standards for heavy duty diesel engines, g/kWh. [22]

Tier	Date	CO	UH	NO_x	PM
Euro I	1992,<85 kW	4.5	1.1	8.0	0.61
	1992,>85 kW	4.5	1.1	8.0	0.36
Euro II	1996.10	4.0	1.1	7.0	0.25
	1998.10	4.0	1.1	7.0	0.15
Euro III	2000.10	2.1	0.66	5.0	0.10
					0.13[a]
Euro IV	2005.10	1.5	0.46	3.5	0.02
Euro V	2008.10	1.5	0.46	2.0	0.02
Euro VI	2013.01	1.5	0.13	0.4	0.01
a - For engines of less than 0.75 l swept volume per cylinder and a rated power speed of more than 3000 rpm					

Table 3 - EU emission standards for passenger cars, g/km. [22]

Tier	Date	CO	UHC+ NO_x	NO_x	PM
Euro I	1992.07	2.72	0.97		0.14
Euro II, IDI	1996.01	1.0	0.70		0.08
Euro II, DI	1996.01[a]	1.0	0.90		0.10
Euro III	2000.01	0.64	0.56	0.50	0.05
Euro IV	2005.01	0.50	0.30	0.25	0.025
Euro V	2009.09	0.50	0.23	0.18	0.005
Euro VI	2014.09	0.50	0.17	0.08	0.005
a-Until 1999.09.30 (after that date DI must meet IDI limit)					

correlations can be used to relate the filtered smoke number to the mass fraction of soot. [23-26]

Nitrogen oxides

The standard technique for NO_x measurements is ChemiLuminescence Detection (CLD). Ozone (O_3) that is generated by the CLD instrument reacts with NO resulting in electronically excited NO_2 and O_2. When the NO_2 returns to its ground state a photon with a wavelength between 600 and 3000 nm is released. Detection of the radiation is made on a photomultiplier and the signal is proportional to the NO concentration. Since the CLD process only detects NO, the NO_2 in the exhausts is catalytically converted to NO and then measured. Detection before and after the instrument's catalytic converter corresponds to NO and total NO_x respectively. The difference between NO_x and NO is then equal to the NO_2 concentration. The CLD has to be calibrated using a known NO and NO_2 concentration regularly. [23,25,26]

Unburned hydrocarbons

UHC can be measured with Flame Ionization Detectors (FID). The exhaust is burned in a carbon-free flame, normally hydrogen-helium, and fed between two electrodes with an applied voltage. The UHC in the exhausts result in ionized carbon and free electrons. The carbon ions are positive and are thereby drawn to the negative electrode. The resulting current is proportional to the number of carbon atoms in the UHC. The FID has to be calibrated with a gas containing zero UHC, for example Nitrogen, and a gas containing a known UHC concentration regularly. [23,25,26]

CO and CO_2

An instrument suited for CO and CO_2 detection is a Non-Dispersive InfraRed (NDIR) analyzer. The instrument measures the absorption of certain InfraRed (IR) wavelengths in the exhausts. It consists of one sample cell, one reference cell and one detector cell, see Fig. 4. A flow of exhaust goes through the sample cell and the reference cell contains air. The sample and reference cells are illuminated with IR radiation and the transmitted radiation is detected. The detector consists

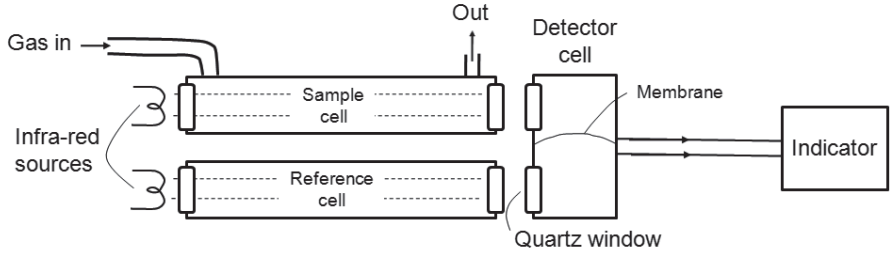

Figure 4 - NDIR gas analyzer. [23]

of a third cell filled with the gas that is to be measured, CO or CO_2. The detector cell is divided into two parts with a membrane in between. One side of the membrane collects the transmitted radiation through the sample cell and the other collects the transmitted radiation through the reference cell. If the exhausts contain the analyzed gas the sample cell will absorb some of the radiation. The sample cell side of the detector cell will then collect less radiation. The gas on the different sides of the detector cell will expand in proportion to the absorbed radiation. The membrane will thereby bulge into the sample side of the detector and the bulge is in relation to the concentration of the measured gas. Beers law,

$$T_\lambda = e^{-\rho\alpha_\lambda L} \tag{20}$$

gives the relation between the portion of transmitted radiation T_λ, the density ρ, the absorptivity a_λ, and the path length L. Eq. 20 is used to relate the transmitted radiation to the concentration of the analyzed gas (CO or CO_2). Some systems use a solid state IR detector instead of the detector cell described here. The NDIR has to be calibrated using a gas containing zero CO and CO_2, for example Nitrogen, and a gas containing a known CO and CO_2 concentration regularly. Optical filters can be used to eliminate the importance of absorption from gases with interfering absorption spectra. [23,25,26]

Chapter 3

Combustion in diesel engines

3.1 Basic concepts

In diesel or Compression Ignition (CI) engines the fuel is introduced and auto-ignited late in the compression stroke. The load in diesel engines is controlled by means of the amount of fuel injected and the combustion phasing is controlled with the fuel injection timing. Diesel engines can be both direct and indirect injected. Indirect injected diesel engines are equipped with a pre-chamber adjacent to the main combustion chamber. During the compression the charge is forced into the pre-chamber and the rather small entrance generates high fluid velocities. The fuel is introduced into the pre-chamber and the turbulent charge provides rapid fuel air mixing [12]. However, today the Direct Injected (DI) diesel engine is the clearly dominating type and the pre-chamber diesel will therefore not be thoroughly described here.

In DI diesel engines the fuel is injected directly into the combustion chamber late in the compression stroke. The fuel spray goes through atomization (break up into droplets), mixes with air, evaporates, and self ignites due to the high ambient temperature. The first step, where the fuel breaks up into droplets, is very rapid in modern diesel engines [27]. The most downstream portion of the spray where fuel droplets occur is called the liquid penetration length. DI diesel engines work with high injection pressures, for example the Scania XPI system uses up to 240 MPa [28]. The charge can be pure air or air mixed with EGR.

Since the diesel fuel is introduced shortly before the combustion, the mixing of fuel and charge gases is not complete before the combustion starts. A central concept in diesel combustion theory is the equivalence ratio, Φ. It denotes the actual fuel-air mass ratio divided by the stoichiometric fuel-air mass ratio

$$\Phi = \frac{\left(F/A\right)_{actual}}{\left(F/A\right)_{stoichiometric}} \tag{21}$$

When the fuel and air mixture is stoichiometric there is just enough oxygen to oxidize all the fuel and $\Phi=1$. In diesel combustion the fuel elements burn with a great variety of Φ values. Fuel elements that initially burn in a fuel rich environment can later be mixed with fresh charge and be further oxidized.

Much of the current diesel engine research aims at decreasing the engine-out pollutants. Since the diesel combustion is a complex process the methods can be very different even if the goal is the same. The same hardware can produce a completely different combustion characteristic depending on the settings. This is utilized in different combustion concepts to minimize the pollutant formation. The main focus in diesel engine development has been to decrease the engine-out soot and NO_x emissions. One way to achieve this is by keeping the combustion temperature low and methods based on this are called Low Temperature Combustion (LTC) concepts [29].

A great variety of LTC concepts has been presented in the literature. Nissan Modulated Kinetics (MK) uses late injection, high swirl, and high EGR levels [30,31]. Swirl is an organized fluid motion around the cylinder axis which can be used to enhance the late-cycle oxidation [12,23]. The Toyota UNIform BUlky combustion System (UNIBUS) uses early injection timings or split injections to facilitate the fuel-air mixing [32]. Other proposed concepts are Partially Premixed Combustion (PPC) [33,34], Premixed Compression Ignition (PCI) [35], and Partially Premixed Compression Ignition (PPCI) [36,37]. All those concepts use high EGR levels and early injection timings to achieve high dilution and a low combustion temperature. The EGR works as a bulk gas that absorbs heat without participating in the reactions. The drawback with low temperature combustion is elevated CO and UHC emissions [29].

3.2 Typical heat release

Much information about the combustion event can be extracted from the calculated heat release rate. Figure 5 shows the heat release rate from a diesel engine. After Start Of Injection (SOI) a negative heat release rate is evident. This is because the fuel evaporation takes heat energy from the ambient charge which lowers the in-cylinder pressure and temperature. This first period is called the ignition delay. Next follows a high rate of heat release. When ignition occurs the available combustible fuel and air mixture burns rapidly. This is called the premixed combustion phase. The premixed phase is controlled by chemical kinetics and the reaction speed depends to a great extent on the temperature [7,18]. The portion of premixed combustion is larger at lower loads and when EGR is used. Later follows the mixing controlled period where the mixing process limits the combustion rate. During the first spray-driven part, the fuel burns as it is injected, evaporated, mixed with air and ignited. After the End Of Injection (EOI) the late combustion phase takes place. The phases are however not

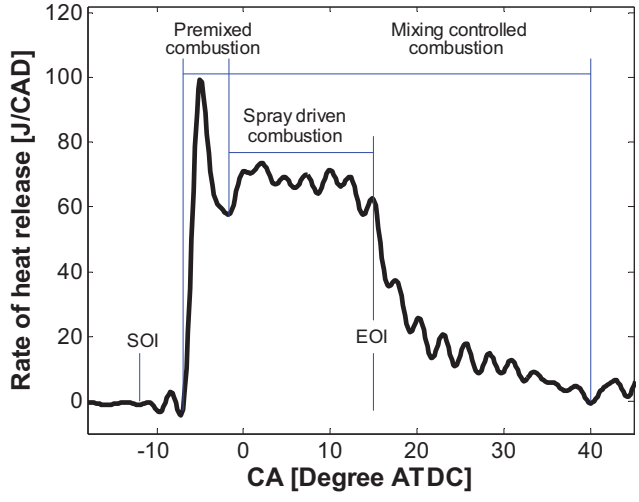

Figure 5 - Phases of diesel combustion as function of Crank Angle (CA) in degree After Top Dead Center (ATDC).

distinctly separated. During the premixed phase, for example, a part of the combustion is mixing controlled. The end of the spray-driven combustion depends on the injector; a fast closing injector gives a distinct transition while a slow closing injector gives a smooth transition to the late combustion.

3.3 The combustion event

Although heat release analysis is a helpful tool, it does not give a detailed understanding of the processes inside the burning diesel jet. Diagnostics on optical engines and pressure vessels, on the other hand, provide the opportunity to follow every part of the combustion process in detail. Accordingly, optical diagnostics has given much of the present understanding of diesel combustion.

In 1997 John Dec presented combined laser-sheet measurements that studied the phases of diesel combustion in detail. The outcome was a conceptual model that gave a new understanding of the course of events inside a reacting diesel jet [38]. In summary, the liquid fuel mixes with air, evaporates, and forms a combustible fuel-air mixture. When auto ignition occurs the mixture burns rapidly, this is the premixed combustion phase in Fig. 5. This phase tends to form soot if the local Φ is higher than 2 [39]. After a while the jet stabilizes and forms certain zones that describe the steps of mixing and reactions for injected fuel elements. Figure 6 illustrates the course of events during this combustion phase referred to as the quasi-steady jet phase. Inside the jet, a zone of fuel-rich premixed combustion stage is formed. The fuel goes through partial combustion and forms soot precursors such as Polyaromatic Hydrocarbons (PAH). Small nuclei are then

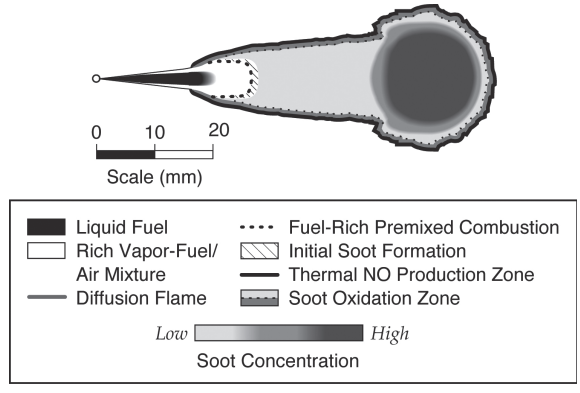

Figure 6 - A schematic showing Dec's conceptual model of DI diesel combustion. Adopted from [38].

formed which grow into primary soot particles. These stick together and form agglomerates as they move downstream in the jet. The amount of fuel that goes through the steps of soot formation and oxidation depends strongly on the operating condition [40,7]. Near the leading part of the jet the soot concentration reaches a maximum. The jet is surrounded by a high-temperature diffusion flame burning at near stoichiometric conditions. This zone forms NO_x and OH, most of the soot oxidation takes place here as well [7].

The influence of engine settings

Since the groundbreaking work by Dec, the conceptual model has worked as an ideal image in the further analysis of diesel combustion. However, the length scales of the different zones shift significantly during different operating conditions. The picture will be affected by injection pressure, EGR, jet-wall interaction, swirl, and nozzle hole size [38].

The most important factor for the flame structure is the mixing process between fuel and air. The rate of entrained hot-air determines the temperature, the evaporation, the first reaction stage, and thus the characteristics of the combustion process. Parameters known to enhance the air-entrainment in diesel sprays are increased ambient density and smaller nozzle orifice diameters. The EGR level does not affect the total gas entrainment but a higher EGR level implies a lower O_2 fraction. Therefore EGR will decrease the O_2 entrainment into the spray. An increased injection pressure increases the air entrainment over time but the speed of the spray is also increasing. The net effect of injection pressure on air entrainment over a given distance is therefore not large. [27,41]

Naber and Siebers have derived a relation between Φ and the distance from the injector orifice [41,27]. The expression was derived applying conservation of mass and momentum principles to an idealized model of a jet. The model assumes a

constant spreading angle, α, radially uniform velocity and fuel concentration profiles, and no velocity-slip between the injected fuel and the ambient gas. According to this simplified analysis, Φ varies as

$$\Phi(x) = \frac{2\left(A/F\right)_{st}}{\sqrt{1+16\left(\frac{x}{x^{+}}\right)^{2}}-1} \tag{22}$$

where $(A/F)_{st}$ is the stoichiometric air-fuel ratio, which is approximately 15 for diesel fuel. The denominator contains the axial location, x, and the characteristic length, x^{+}, that is used to simplify the expression.

$$x^{+} = \sqrt{\frac{\rho_f}{\rho_a}}\,\frac{d\sqrt{C_a}}{\tan\left(\alpha/2\right)} \tag{23}$$

where ρ_f and ρ_a are the fuel and ambient gas densities, respectively. The area contraction coefficient, C_a, and the hole diameter, d, are related to the nozzle geometry. The jet spreading angle, a, depends on the fuel and ambient gas densities.

The most upstream part of the burning diesel flame is called the lift-off position and is commonly determined from OH-chemiluminescence. The lift-off position, H, follows the empirically established relationship

$$H \propto T_a^{-3.74}\rho_a^{-0.85}d^{0.34}UZ_{st}^{-1} \tag{24}$$

where T_a is the ambient temperature, U the fuel velocity, and Z_{st} is the stoichiometric mixture fraction, which is the ratio of the fuel mass to the total mass at stoichiometric conditions [42].

After the lift-off position the air entrainment into the center of the jet is aggravated since the oxygen is consumed by the reactions on the surface of the flame. The local Φ in the lift-off region is thereby important for the combustion characteristics and the emissions formation. The soot forming process during the quasi-steady jet phase in particular is thought to be affected by the air entrainment upstream the lift-off position [43-49]. Although the usage of EGR changes the jet structures to a great extent, it does not necessarily have a net effect on the equivalence ratio in the lift-off zone [43,44,50]. This is due to two counteracting trends. The lower ambient O_2 fraction gives less O_2 entrainment over a given distance. The lift-off position however moves downstream at the

same time, which potentially gives the same oxygen entrainment up to the lift-off position.

An extended version of the conceptual model was presented by Mark Musculus in 2006 [48]. It describes the burning diesel jet during low temperature combustion with high EGR levels and early injection timings. When high levels of EGR are introduced the structure of the flame is changed. The soot production is moved downstream and does not start before the head of the jet. The OH and NO production zones are moved inside the jet and occurs over the whole jet cross section.

Pollutants from diesel engines

Two of the most important pollutants from diesel engines are NO_x and PM. A significant contribution to PM comes from combustion generated soot particles.

Soot is formed in hot fuel-rich combustion zones while the soot oxidation is most efficient during high temperature, lean conditions, and high turbulence. If the equivalence ratio at the lift-off position is reduced it possibly suppresses the soot-formation during the jet-phase. This is commonly desired in proposed, modern diesel combustion concepts. It is however hard to affect the soot forming without affecting the soot oxidation. Factors that impede soot-formation might also aggravate soot oxidation. Therefore, even if the soot forming is suppressed it is not obvious that the engine-out soot will decrease.

NO_x can be formed from either atmospheric nitrogen or nitrogen from the fuel by different mechanisms [12,51]. The major portion of NO from diesel engines is generally formed by the so called thermal mechanism. The principal reactions leading to thermal NO formation from atmospheric nitrogen are;

$$O + N_2 \rightleftharpoons NO + N \tag{25}$$

$$N + O_2 \rightleftharpoons NO + O \tag{26}$$

$$N + OH \rightleftharpoons NO + H \tag{27}$$

The two upper reactions were first suggested by Zeldovich and the lower one was added by Lavoie *et al.* [12]. The NO can be further oxidized to NO_2. Eq 25-27 are reversible and the equilibrium NO concentration is higher at higher temperatures. The reaction speed is highly temperature dependent and the concentration freezes during the expansion stroke when the temperature drops. Most of the formed NO_x therefore ends up in the exhausts and factors that impede the NO_x formation give less engine-out NO_x. The in-cylinder temperature and thereby NO_x formation is linked to the combustion phasing. An early phased combustion gives high temperatures over a long time period and a high NO_x formation. A late phased

combustion gives low NO_x formation and thus a low engine-out NO_x concentration. For diesel combustion without EGR the NO_2 fraction of the engine-out NO_x is low but increases with the dilution level and can be above 80% at low O_2 mole fractions [52]. The increased NO_2 fraction at lower O_2 fractions is thought to arise from increased quenching of NO_2 to NO reactions due to decreasing flame temperatures. [52,12]

A useful picture of the formation of the soot and NO_x in diesel engines is presented in [18]. Figure 7 shows the temperature and equivalence ratio dependence on soot and NO_x production. Figure 7 is generated from homogeneous reactor simulations, meaning that it shows the results of reaction at constant temperatures and equivalence ratios. The reaction time is 2.0 ms. NO_x needs a high combustion temperature, >1800 K, to form and is absent at richer zones than Φ=2.5. The area of soot production is well separated from NO_x and takes place at Φ>2 and peaks around 1900 K. The unfilled arrows in Fig. 7 corresponds to a simplified description of the path for a typical fuel element during classic diesel combustion without EGR. The fuel element starts at low temperature and high equivalence ratio. As it mixes with air, the equivalence ratio decreases and the temperature increases. When ignition occurs the temperature increases at a fairly constant equivalence ratio and the fuel element enters the soot-formation area. As the fuel is consumed, the mixing with oxygen continues and the equivalence ratio decreases further. The temperature increases and the NO_x formation starts. The peak combustion temperature is reached at an equivalence ratio slightly above 1. After this point both the equivalence ratio and the

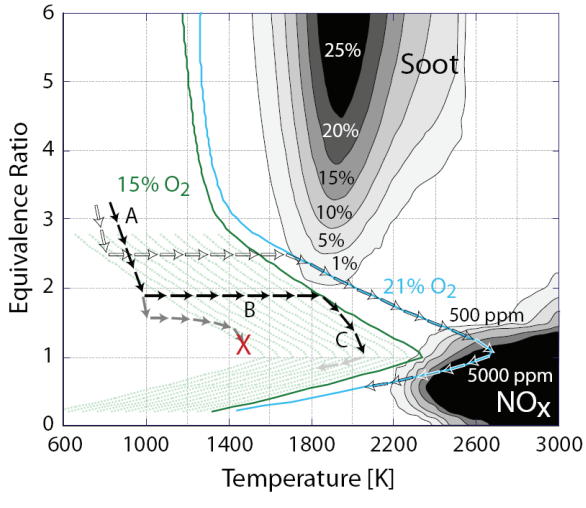

Figure 7 - Soot and NO production zones as function of temperature and equivalence ratio. The yield is obtained from a homogeneous reactor simulation of an n-heptane/air mixture during 2.0 ms. The adiabatic flame temperature is shown by the turquoise line at 21% ambient oxygen concentration, and the green line at 15% ambient oxygen concentration. [18]

temperature decreases. In reality the picture is far more complex since different fuel element ignites at a great variety of temperatures and equivalence ratios .

The Φ/T zone with high NO_x formation in Fig. 7 provides good conditions for soot oxidation. Accordingly, if the conditions for NO_x formation are suppressed the soot oxidation process is aggravated. The result is a trade-off between soot and NO_x emissions that can be challenging for engine manufacturers to break. There are two main paths to achieve simultaneous reduction in soot and NO_x emissions: 1) A sufficient soot oxidation late in the cycle when it is too cold for NO_x formation and 2) suppressed combustion temperatures that simultaneously avoid soot and NO_x formation. The second alternative is the goal with LTC concepts. This is shown by the black arrows in Fig. 7. The drawback is however elevated emissions of CO and UHC.

To illustrate this, an extended version of Fig. 7 is presented in Fig. 8 [37]. This image shows the fraction of CO and UHC after 2 ms reaction time in addition to soot and NO_x. The yields of CO and UHC have many similarities but also some differences. Both CO and UHC can originate from lean and rich mixtures. For lean mixtures, a high CO yield is present when temperatures are between 800 K and 1400 K, while in rich mixtures CO is produced at all temperatures above 800 K. Below 800 K the fuel does not ignite resulting in 100% UHC. At lean mixtures above 1200 K most of the UHC is converted in to CO or completely oxidized. At rich mixtures a high UHC yield is present up to approximately 2000 K. Above this temperature most of the incompletely oxidized fuel end up in CO. [37]

Unlike CO, which is formed by partial fuel oxidation, UHC does not need to be formed. The number of carbon atoms in the UHC molecules contains information about the source. Heavy UHC components are thought to be linked to liquid fuel

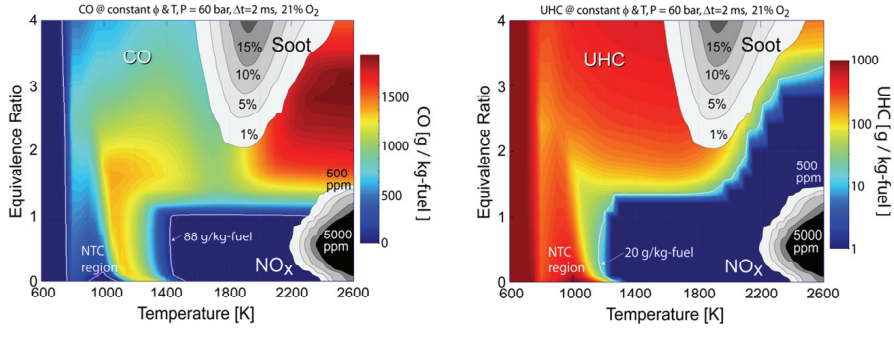

Figure 8 - NO_x and soot yield as function of equivalence ratio and temperature. The left figure is extended with the CO yield and the right figure is extended with the UHC yield. The yield is obtained from a homogeneous reactor simulation of an n-heptane/air mixture. The ambient pressure is 60 bar and the reaction time is 2.0 ms. [37]

that never gets the chance to react. This can be liquid injector dribble during expansion or liquid fuel films that survive the combustion. Lighter UHC components stem from partially oxidized fuel and are coupled to the same sources as CO. [53-56]

The above understanding of diesel combustion can be used to control the combustion event in order to decrease the engine-out emissions. The challenge is to avoid zones with high formation, or enhance the oxidation of pollutants. This is however not easily achieved since the individual fuel elements burn with a high variety of equivalence ratios and temperatures.

Chapter 4

Results and discussion

The results included in this thesis can be divided into two main categories: one about evaluations of optically accessible engines and one about emissions formation. The reason for putting efforts on the first category is to get more reliable information from the second one. The section about emissions is divided into two sub sections: one about soot and one about of CO and UHC.

4.1 Evaluation of optical engines

Mechanical deformation

Combustion engines are exposed to forces from high pressures, thermal expansion, and acceleration due to the piston movement. These forces have an impact on the engine structure, causing stresses and vibrations. When designing engines, these have to be considered to obtain a durable and usable engine. However, the forces also result in a distorted in-cylinder volume trace since different engine parts expand or become compressed due to the forces. The effects are present in all engines but are more severe in optical engines since both the piston and engine block are extended, see Fig. 1. The deformations are expected to have a rather small influence on the combustion process if changes in TDC conditions are compensated. However, since the in-cylinder volume and its derivative are essential for pressure analysis it is useful to quantify them precisely. This section discusses the impact of the deformations on the heat release analysis. The deformations were quantified with measurements of the squish height during motored operation with high speed video. The result presented is acquired on Engine 1 in Table 1 but the deformations has also been studied on Engine 2 and 4.

The thermal forces act to expand the engine parts as they increase in temperature during operation. The acceleration forces expand the moving parts near TDC while they compress them near Bottom Dead Center (BDC). The pressure forces are largest near TDC and act to compress the moving parts while they expand the engine block and the engine block extension. The in-cylinder volume near TDC will thereby be increased by gas forces while it will be

decreased by mass forces. The thermal expansion affects the compression ratio which affects the in-cylinder volume but it does, in contrast to mass and pressure forces, not affect the volume derivative.

The distortion from mass and pressure forces could be compensated by rewriting the equation for the in-cylinder volume as function of CAD.

$$V_{adjusted} = V + \frac{\pi B^2}{4}\left(p(\vartheta)k_p - a_{osc}(\vartheta)k_a\right) \tag{28}$$

where V is the volume according to Eq. 2, B is the cylinder bore, $p(\vartheta)$ is the pressure as function of CAD, k_p and k_a are the deformation constants due to pressure and piston acceleration. k_p should contain the axial deformation plus the relative importance of the radial deformation. Furthermore, a_{osc} is the oscillating acceleration according to [13],

$$a_{OSC} = r_{crank}\omega^2\left(\cos\vartheta + \lambda\cos 2\vartheta\right) \tag{29}$$

where ω is the angular velocity and λ is the ratio between the crank radius, r_{crank}, and the connecting rod.

Such a procedure gave a more reasonable shape of motored rate of heat-release traces independently of pressure level. The motored heat release rate should be slightly negative in the vicinity of TDC since the heat and mass losses are not accounted for here. Figure 9 shows the motored heat release calculated with different volume traces. Black dotted curves use a standard volume trace according to Eq. 2 and blue solid curves use a volume trace adjusted for mechanical deformation i.e. calculated with Eq. 28. As the motored peak pressure increases, the black curves deviate more from zero while the blue curves retain a reasonable shape.

The traditional procedure to account for deviations from the theoretical volume trace is to adjust the compression ratio. Such an attempt is performed in Fig. 10 for the motored pressure trace with the highest peak pressure in Fig. 9. Three motored rate of heat release traces using a standard volume trace from Eq. 2 with different compression ratios are plotted in Fig. 10. In addition, one motored heat release curve using an adjusted volume trace from Eq. 28 is shown for comparison. It can be seen that independently of compression ratio, using Eq. 2 does not lead to a reasonable shape of the rate of heat release for such high motored peak pressure. This is since a changed compression ratio does not affect the volume derivative at a given crank angle position.

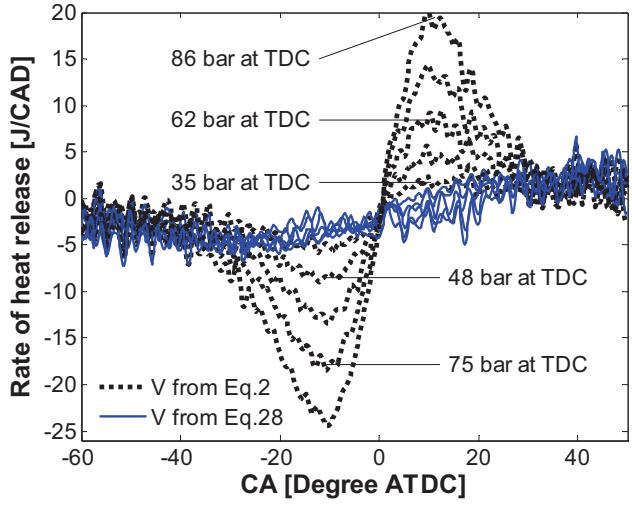

Figure 9 - Motored heat release rate traces for different pressure traces. The dotted curves are calculated with a volume trace according to Eq. 2 using a compression ratio that gives the true clearance volume for a TDC pressure of 34 bar. The solid curves are calculated with volume traces according to Eq. 28. The pressure at TDC are indicated for the black dotted curves.

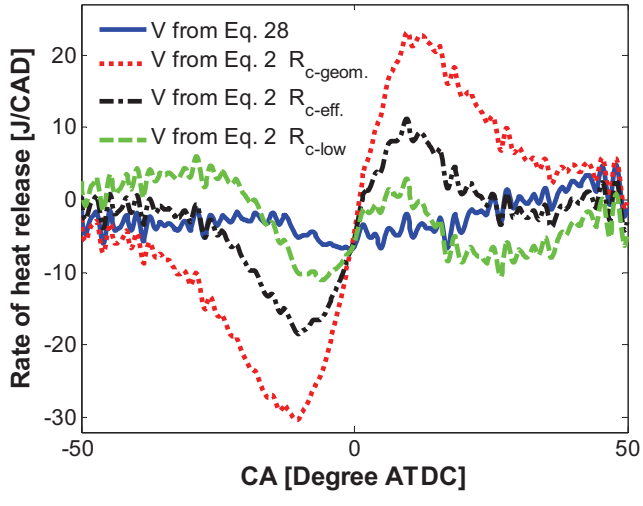

Figure 10 - Motored heat release rate traces, calculated with different volume traces. The volume trace for the red dotted curve is calculated using Eq. 2 with the geometrical compression ratio (16.8). The black dash-dotted curve is based on an effective compression ratio (14.5) at the current peak pressure, 86 bar. The green dashed curve uses an unrealistically low compression ratio (13.2) and is only shown for comparison. The blue solid curve is calculated using Eq. 28.

Heat release calculations for fired pressure traces can be improved with the same method or with a simplified equation and a motored heat release subtraction. A motored and a fired engine, with the same speed and boost pressure, are exposed to equally large pressure forces until the combustion starts and the same mass forces over the whole engine cycle. Figure 11 shows the fired heat release for a pressure trace calculated with different volume traces. The engine load is 6 bar gross Indicated Mean Effective Pressure $IMEP_g$. For all cases except the red curve the motored heat release, using the same volume equation as for the fired pressure trace, is subtracted. It is evident that the usage of Eq. 28 instead of Eq. 2 gives a different shape of the fired heat release even when the motored heat release is subtracted. The premixed and early mixing controlled heat release is underestimated while the late heat release is overestimated if the deformations are ignored. Comparing the solid blue curve with the dashed green curve it is evident that the acceleration part of Eq. 28 does not matter much if the motored heat release is subtracted since the curves are almost overlapping. This simplifies the procedure since only one deformation constant needs to be determined instead of two (i.e. only k_p instead of both k_a and k_p).

The impact from deformations on heat release analysis for Engine 2 and 4 was much smaller than for Engine 1 at a similar load case, see paper VI. However, it was shown that the deformations affect the shape of the heat release even on

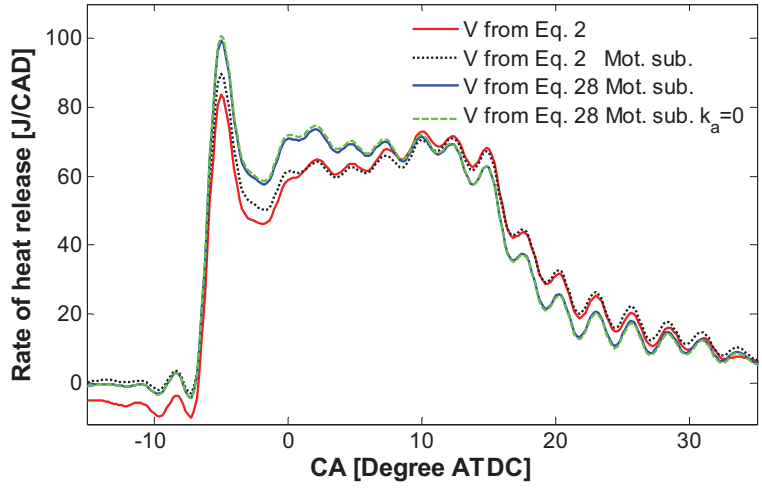

Figure 11 - Four heat release rate traces for a pressure trace calculated with different volume traces. The solid blue curve corresponds to a volume calculation with Eq. 28, the dashed green curve is calculated with Eq. 28 without the term for acceleration. The black dotted and the red curves are from Eq. 2 with an effective compression ratio. For all cases except the red curve the motored heat release calculated with a volume trace using the same method as for the fired pressure trace is subtracted. The load is 6 bar $IMEP_g$.

Engine 4, which is an all metal engine, in cases with steep pressure gradients. The calculated IMEP was not much affected by the deformations on either of the engines.

This investigation of mechanical deformation was the last study performed within the body of this thesis. The knowledge could thereby not be utilized in the other investigations. Since the deformations affect all of the preceding investigations it would have been more suitable if it were performed first. With hindsight, relevant data from earlier investigations will be re-evaluated in this thesis, mainly to establish that the conclusions were sound but also to learn more of how the new insights affect pressure analysis.

Combustion phasing differences

This section analyzes combustion process differences between optical and all-metal engines. The method is to compare the heat release and engine-out emissions between different engine configurations with various degrees of optical access. In the studied combustion case a short injection duration was used. This essentially did not produce any spray-driven combustion i.e. the premixed combustion phase directly evolves into the late combustion phase.

The comparison showed that when operated in the same manner there were differences in the combustion phasing and engine-out emissions between the studied engine configurations. All observed differences were related to lower heat losses in optical engines. Quartz is a much poorer heat conductor than aluminium and steel [57]. Low heat conductivity leads to low heat losses and high wall temperatures which favours a fast ignition with a short ID. The short ID gives little time for fuel and air to mix before the combustion starts which results in a short, early phased premixed combustion with a small portion of the total heat release. This also leaves more energy for the mixing controlled heat release, extending this phase. The shorter ignition delay therefore indirectly leads to a later end of combustion. The early phased premixed combustion leads to elevated NO_x emissions. Furthermore, the higher surface temperature gives a more efficient oxidation resulting in higher combustion efficiency.

The purpose of the investigation was to analyze the differences in combustion characteristics and also to study possibilities to compensate for them. The modification that had the largest impact on both the heat release and engine-out emissions was the piston crown material. The focus is thereby to achieve the same combustion characteristics in a configuration with a quartz piston crown as in a similar configuration with a aluminium piston crown. All the observed differences were related to a change in combustion phasing. Factors known to affect the combustion phasing i.e. EGR level, SOI and inlet temperature, were therefore varied. The parameter that gave the best result was the inlet temperature.

Figure 12 shows the normalized difference between an engine configuration with a metal piston crown and a similar configuration with a quartz piston crown, as function of the ratio in inlet temperature between the configurations (T_M/T_Q). The compared quantities are related to the combustion phasing, the engine-out emissions, and the exhaust temperature. The combustion efficiency contains information of the levels of CO and UHC. For abscissa values from 0.9 to 1 the inlet temperature in the quarts configuration is 388 K while the metal configuration goes from 358 K to 388 K. For abscissa values from 1 and above the inlet temperature in the metal configuration is 388 K while the optical configuration goes from 388 K to 358 K.

When the inlet temperature is 8% lower in the metal configuration (0.92 on the abscissa) there are quite large differences between the configurations, the combustion starts later and ends earlier in the metal configuration. The portion of premixed heat release is higher while the NO_x emissions, combustion efficiency, and exhaust temperature are lower. When the inlet-temperature ratio is increased successively all values approach zero. Finally when the temperature is 8% higher in the metal configuration (1.08 on the abscissa) all measures except the specific NO_x emissions are close to zero. The NO_x mole fraction is very similar between the configurations but since the mass flow ratio decreases when the inlet temperature ratio increases the normalized difference in specific NO_x emissions

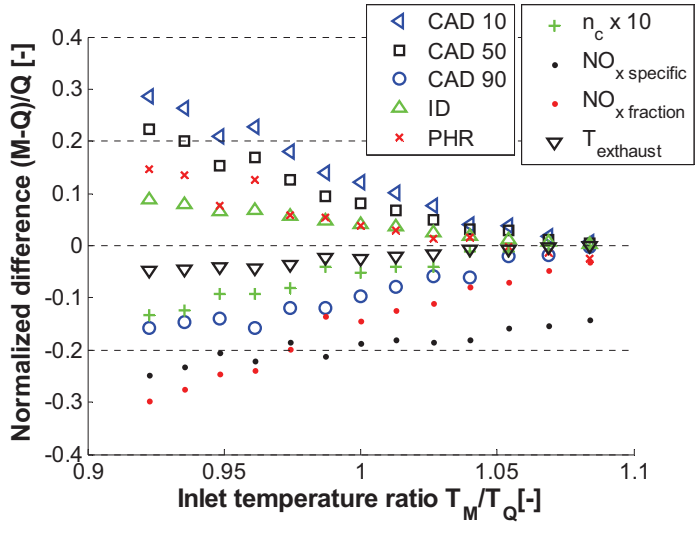

Figure 12 - The normalized difference between two engine configurations i.e. the quantity for an engine configuration with a metal piston crown (M) minus the same quantity for a similar configuration with a quartz piston crown (Q) divided with the quantity for the quartz configuration ((M-Q)/Q). The measures are; CAD at 10% heat release, CAD at 50% heat release, CAD at 90% heat release, portion of premixed heat release (PHR), ignition delay (ID) [CAD], combustion efficiency (difference enlarged 10 times for clarity), specific NO_x emissions [$g/kWh_{indicated}$], NO_x mole fraction [ppm], and exhaust gas temperature [K].

does not reach zero. All quantities, including the specific NO_x emissions, show monotonous trends as function of the temperature ratio which implies that it is no coincidence that it was possible to decrease the differences.

The remaining question is if the difference in specific NO_x emissions means that optical engines always produce higher levels of NO_x. The inlet temperature sweep was performed on three engine configurations, two with a metal piston crown, and one with a quartz piston crown. All three configurations showed a monotonous decrease in specific NO_x emissions with a decreased inlet temperature. Another configuration equipped with a quartz piston crown but with higher compression ratio showed 10% lower specific NO_x emissions than the quartz piston configuration used here (when both configurations were operated with an inlet temperature of 373 K). An engine failure prevented that configuration from being included in the inlet temperature sweep. However, since the three other configurations showed monotonous trends in specific NO_x emissions to the inlet temperature it is likely that this would be the case even for the quartz piston configuration with the higher compression ratio. It is also very likely that the specific NO_x emissions would be far less deviant from the configuration with the metal piston during such a comparison.

Normally optical engines are used for more fundamental combustions studies and the result is not directly related to a specific operating condition on an all-metal engine. It is, however, important to know that the knowledge is transferable since the whole reason for optical engine studies is to understand all-metal engines. The important result of this study is that it is possible to achieve realistic heat release and engine-out emissions in optical engines of Bowditch design.

This investigation was performed before the effects of mechanical deformations were studied. Since the mechanical deformations were shown to have an impact on the heat release calculations, the old data are re-evaluated with respect to deformations. This is important since two different engine structures with different deformation constants are compared here: Engine 2 and 4 in Table 1. The deformation is about twice as large on the optical engine as on the all-metal engine at a given pressure, see paper VI.

The ignition delay evaluation is found to be unaffected by the deformations. For the premixed heat-release there is, however, differences since the height of the premixed peak is underestimated if the deformations are ignored. Figure 13 shows the portion of premixed heat release calculated without regard to deformations in solid lines and with the deformations considered in dotted lines. C1 in Fig. 13 is an all-metal engine and C2 to C5 are different set-ups of an optical engine. Higher configuration numbers are equal to more optical components, see paper I for details. As evident the portion of premixed heat release was underestimated for all cases but since all curves are shifted in the same direction no false

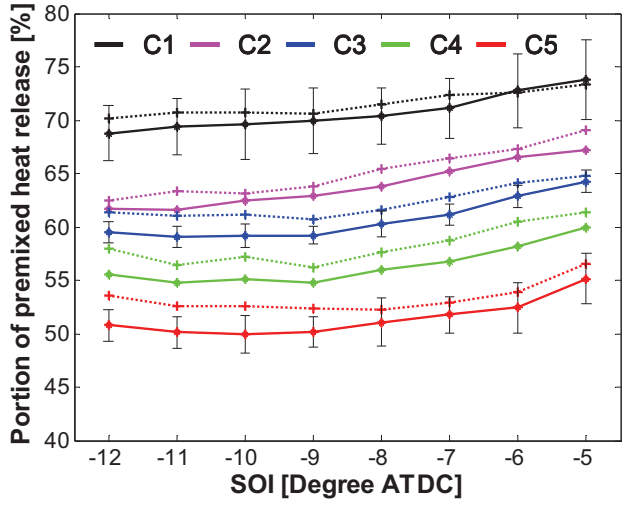

Figure 13 - Portion of heat release in the premixed combustion phase as a function of SOI for configuration 1 (C1) to C5 at 2.4 bar $IMEP_g$. C1 is an all-metal engine and C2 to C5 are different set-ups of an optical engine. Higher configuration numbers are equal to more optical components. The deformations are considered for dashed curves but not for solid curves.

conclusions were drawn. The absolute value of the portion is not as interesting as the difference between the configurations. In paper I, also other aspects of the heat release were compared between the configurations but the portion of premixed heat release was the one that was most affected by the deformations. The reason for the relatively small errors is the low boost pressure, 1.1-1.25 bar, and the low load, 2.4 bar $IMEP_g$.

4.2 Soot processes

The level of engine-out soot emissions is the result of a complex series of events including fuel air mixing, premixed combustion, mixing-controlled combustion, and soot oxidation during both the fuel injection and late in the cycle. The second part of the work presented in this thesis studies factors that are known to be important for the soot-formation process and estimates how they affect the engine-out soot emissions. The goal is to identify characteristics of the soot-formation that are important for the engine-out smoke level and thereby the soot particle mass. Two studies are included in this chapter, one about air entrainment and one about early soot-formation. Both studies are performed on a heavy duty optical engine; Engine 1 in Table 1.

The engine is operated at low load but with long injection duration since prototype nozzles with fewer and smaller holes than normal are used. A three-hole nozzle cup is used in the study about air-entrainment while the soot-

formation study uses a four-hole nozzle cup. The hole diameter is 100 µm in both cases. The number of holes in production engines varies but seven or eight is quite normal and the hole diameter is normally closer to 200 µm than 100 µm for heavy duty engines. The prototype nozzles are used for two reasons: first, to prevent adjacent jets from limiting the optical access perpendicular to the studied jet, and second, to get a large portion spray-driven combustion at a load that can be handled in the optical engine.

Even if the studies use slightly different hardware they essentially investigate the same combustion case and the results are thereby directly compared in the discussion below. The studied load is 6 bar $IMEP_g$ and the baseline properties feature an injection pressure of 2000 bar, an ambient O_2 mole fraction of 14% and a TDC density of 27 kg/m^3. For details see papers II and IV.

Air entrainment

In the first study, the local Φ in the lift-off region was compared with the engine-out soot particle mass. A central concept of the discussion below is the quasi-steady jet phase. This phase is defined as the period from when the upstream position of the diesel jet zones described by Fig. 6 stabilizes until the EOI. The local Φ at the lift-off position is thought to be important for the rate of soot-formation during this phase. This is since the diffusion flame surrounding the jet consumes most of the oxygen entrained downstream of this position which strongly limits the reduction rate of the equivalence ration in the interior of the jet. The lift-off length was determined from line of sight OH-chemiluminescence images and the local Φ value in the interior of the jet was measured with Raman spectroscopy. The experimental variables were the injection pressure, the ambient density at TDC, and the inlet O_2 mole fraction. The settings of the variables are given in Fig. 14.

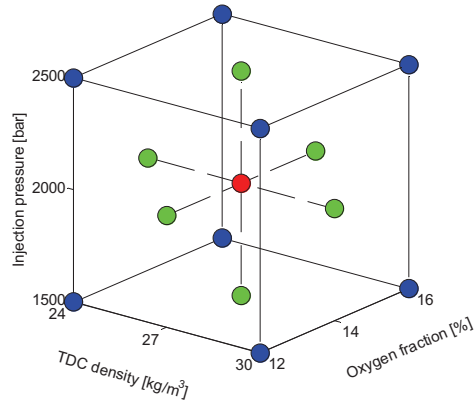

Figure 14 Graphical representation of the experimental factors and their levels.

The study was divided into two parts; one that studied the engine-out emissions and lift-off position and one that studied the air entrainment in the jet. The air entrainment study was performed in a non reacting jet. This is since it was not possible to measure the equivalence ratio inside a reacting jet with the selected measurement technique. Since the spacing between the jets is 120 degrees it is assumed that the gas entrainment up to the lift-off position is mainly fresh charge. The equivalence ratio at this position might thereby be similar as for a reacting jet. However, the impact of turning off the combustion is hard to estimate and the focus should be on the trends rather than absolute values of the equivalence ratios.

Measurements of Φ were made at the same axial position for all compared cases and scaled to the lift-off position using Eq. 22. The Φ values at lift-off were then compared with the engine-out soot emissions. Figure 15 shows the combined effect of injection pressure and O_2 mole fraction on engine-out soot emissions and Φ at lift-off. The trends in soot emissions and Φ at lift-off are far from similar. The soot emissions decrease with increasing oxygen fraction and injection pressure. Φ at lift-off shows no consistent trend with the injection pressure and when the oxygen fraction is varied a local minimum is evident at approximately 14% O_2 at all injection pressures. Besides Φ at lift-off the soot forming rate is also affected by the flame temperature as can be seen in Fig. 7. At a given equivalence ratio the flame temperature increases with oxygen mole fraction since each fuel element has a smaller mixture mass to heat. The soot forming rate should thus be the highest at high Φ values and high oxygen fractions. The position where the highest soot forming rate is expected is indicated with the red oval in the right contour plot in Fig. 15. However, the left contour plot in Fig. 15 shows that engine-out soot emissions are zero at this position. If the soot forming rate during the quasi-steady jet phase was determining for the engine-out soot emissions, the plots for soot emissions and Φ at lift-off would show similar trends. High soot emissions would also be expected at the highest soot forming rate. This is clearly

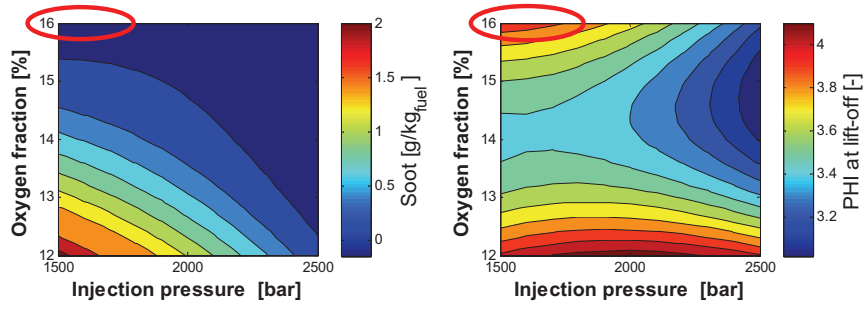

Figure 15 - Contour plot of Φ at lift-off and engine-out soot emissions. The graphs show the combined effect of injection pressure and O_2 mole fraction. The red oval indicates where the highest soot forming rate is expected.

not the case. To further quantify this lack of relation, a correlation analysis was performed. Figure 16 shows the absolute values of correlation coefficients between soot emissions and parameters that are thought to be connected to the soot-formation or soot oxidation processes. The parameters are; Φ in the measurement point, Φ at the lift off position, the lift-off position, engine-out UHC, engine-out CO, and the portion of heat released after the end of injection.

After EOI the kinetic energy and turbulence provided by the spray gradually dissipates. It is therefore reasonable to assume that the oxidation rate decreases after EOI. The portion of heat released after EOI could thereby provide information about the inefficiency of the soot oxidation process. The engine-out emission levels of CO and UHC also gives information about the oxidation process since these emissions are the result of insufficient oxidation. Φ in the measurement point, Φ at the lift off position, and the lift-off position are thought to contain information about the soot-formation process.

For a sample size of 15 the correlation coefficient should exceed 0.45 to be statistically significant, based on a one-tailed t-test with the confidence level of 95% [58]. The only factors showing a significant correlation is the heat released after EOI, the engine-out CO and the engine-out UHC. Φ at the lift-off position has a surprisingly low correlation coefficient, even lower than the measured Φ. In contrast, the bars in Fig. 16 suggest that the soot oxidation process may be more important for engine-out soot emissions than the soot forming rate during the quasi steady jet-phase.

This investigation was performed before the study about mechanical deformations

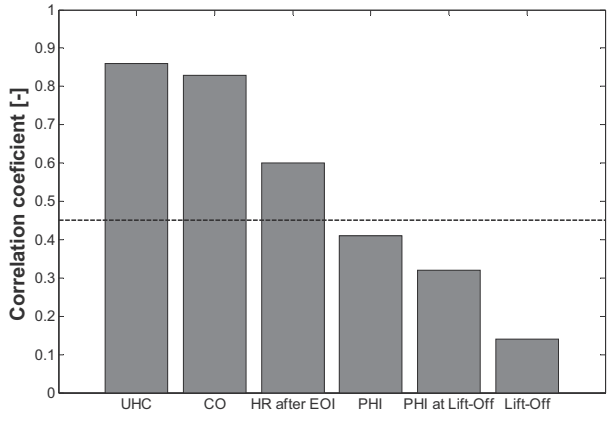

Figure 16 - Correlation coefficients between engine-out soot particle mass and different parameters. The UHC and CO emissions has the unit g/kg_{fuel}. The dashed line indicates the level that the correlation coefficient should exceed to be statistically significant, based on a one-tailed t-test with the confidence level of 95%.

(presented in section 4.1) and the heat release analysis thereby did not account for the associated distortion of the in-cylinder volume trace. As can be seen in Fig. 11, the mechanical deformations were found to have rather large impact of the shape of the heat release of the heavy duty optical engine (Engine 1 in Table 1), where the air entrainment was studied. Since the deformations were ignored, the early heat release was underestimated while the late heat release was overestimated. This also means that the heat release after injection was overestimated. When the heat release had been re-evaluated with respect to deformations, the portion of heat release after the end of injection decreased for all cases but the decrease was quite monotonous. The correlation coefficient between the heat release after injection calculated with and without deformations is 1.0 (0.9971). The conclusions would thereby not be different if the deformation had been considered from the beginning.

Early soot-formation

In the air entrainment study above the O_2 mole fraction largely affected the equivalence ratio at the lift of position but the impact was far from linear. In order to better understand this behaviour the early soot-formation as function of O_2 mole fraction was studied. Time-resolved LII using 8 laser pulses with a spacing of one CAD was utilized to qualitatively follow the soot-formation process in one of the jets from start of combustion to CA50. The laser sheet was tilted with the same angle as the jet axis to be able to capture the evolution of the soot distribution in the interior of the jet. The test matrix consisted of a sweep of inlet O_2 mole fraction between 9 and 21%.

Figure 17 shows the engine-out emissions of smoke. As the O_2 fraction was lowered from 21 to 9%, the engine-out smoke level increased from zero FSN up to a peak of 2 FSN, occurring between 11 and 12% O_2, from where it decreased down to almost zero again at 9% O_2.

Figure 18 shows the initial soot distribution in the jet at 10, 14, and 21% inlet O_2 fraction. At 21% the first soot is formed upstream of the wall. The soot cloud then grows and reaches the wall where small recirculation zones are formed. For the 14% O_2 case, the soot starts to form at the wall. The soot cloud follows the curvature of the bowl wall as it grows in the subsequent images. Signal levels are initially low but increase in the recirculation zones, indicating a stronger soot formation in these regions. At 10% O_2 the soot starts to form in the recirculation zones between adjacent jets. The signal is weaker than in the other cases. Figure 19 shows the energy content in the premixed, spray-driven and late phase of the heat release rate as function of inlet O_2 fraction.

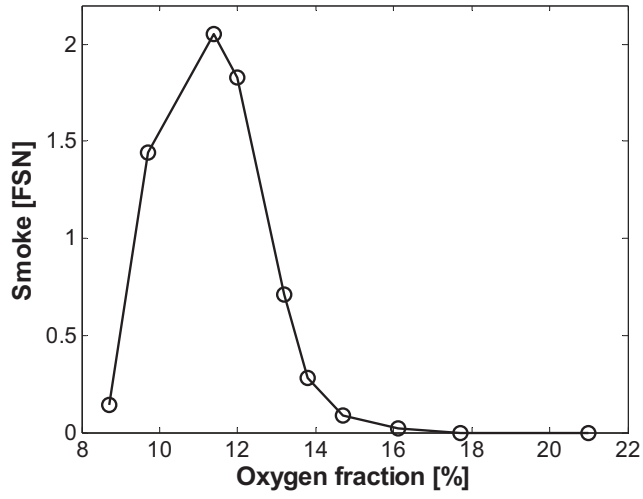

Figure 17 - Engine-out emissions of smoke as function of inlet O_2 mole fraction.

Figure 20 shows when the soot-formation starts in relation to these heat release phases. The first soot appearance is closely connected to the start of the spray-driven heat release phase for all O_2 fractions. Recall that a nozzle with fewer and smaller holes than normal is used in order to get a large portion spray-driven heat release. The spray driven combustion phase reaches a maximum of 70% at 21% O_2. When the O_2 fraction is lowered the energy content in the spray-driven combustion decreases while it increases in the premixed and late combustion phases. The injection duration is 27 CAD, determined from Mie scattering.

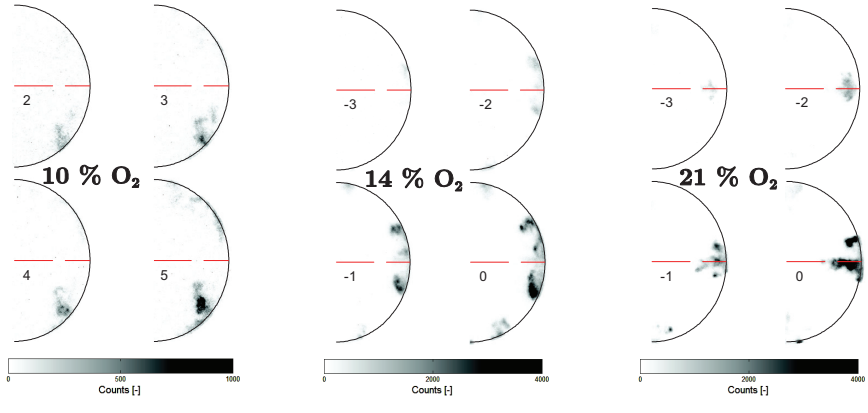

Figure 18 - Initial soot distribution for, from left to right; 10, 14, and 21% inlet O_2 mole fraction. The numbers in each image indicate the crank angle degree after TDC, the dashed line indicates the jet axis.

Even if the transition between the premixed and mixing controlled combustion is distinct in the rate of heat release curve the reality is that a part of the premixed combustion phase is mixing-controlled and a part of the mixing-controlled phase is premixed. When looking at the time-resolved soot measurement in Fig. 18 it is evident that the jet is far from stationary at the start of the spray-driven combustion since all images are acquired during this combustion phase. After the start of soot-formation, it takes several CAD:s before the most upstream position of the soot cloud stabilizes. At the peak in engine-out smoke, 11.4% O_2, the portion spray-driven combustion is approximately 45% while the premixed portion is just below 20% as shown in Fig. 19. Figure 20 gives that the start of spray-driven combustion and first soot appearance occurred midway through the injection event for this O_2 fraction (determined from Mie scattering). Accordingly, approximately 50% of the fuel is injected but only 20% of the heat-release is completed at the start of soot-formation. This leaves approximately 30% of the total fuel energy in incompletely oxidized mixtures.

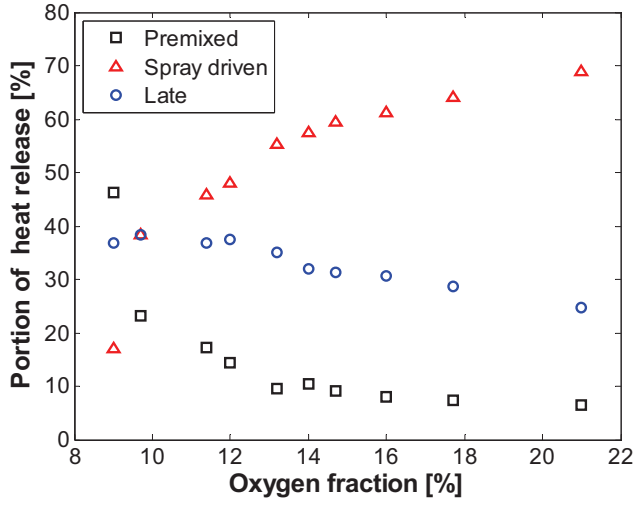

Figure 19 - Energy content in the premixed, spray-driven and late phase of the heat release rate as function of O_2 mole fraction. The heat release is calculated using a volume trace according to Eq 28 and heat losses according to Eq:s 17, 18, and 19.

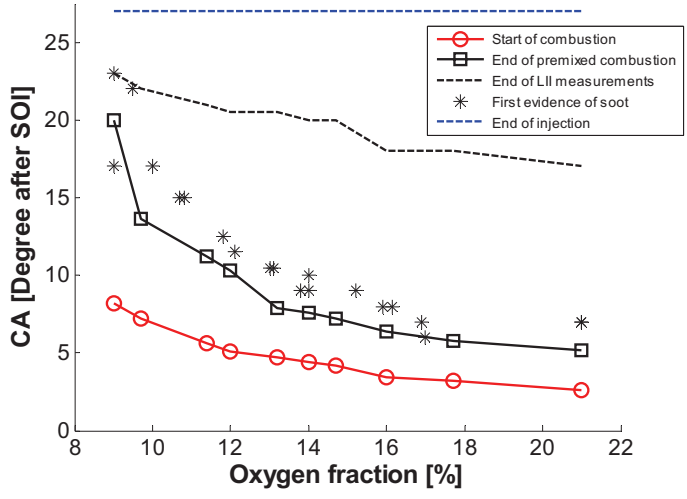

Figure 20 - Start of combustion, end of premixed combustion, time for the first soot appearance, and end of injection as function of inlet O_2 mole fraction. All values expressed as CAD after SOI. The heat release is calculated using a volume trace according to Eq 28 and heat losses according to Eq:s 17, 18, and 19.

A certain portion of this fuel is in the spray upstream the flame but the major part has plausibly travelled further downstream since the fuel injection has progressed for 13 CAD. Furthermore, moderately lean or stoichiometric regions are likely to be close to fully O_2 during the premixed combustion. Zones of mixtures too lean to burn may exist but presumably do not contain a great portion of the total fuel energy. Quantitative equivalence ratio measurements done by other investigators show that the clearly dominant portion of the mixture is fuel rich at start of combustion independently of ambient O_2 fraction [43]. It is thereby likely that the major fraction is trapped in partially-oxidized fuel-rich zones in the interior of the flame. The history of mixing for this fuel quantity is different from a stationary jet since most of the mixing has occurred before the positions of the jet is formed. It is thereby reasonable to assume that the air entrainment upstream the lift of position is of less importance for this fuel quantity than for fuel combusted in a stationary jet.

To be able to compare the soot-formation with the engine-out smoke in greater detail, key values were extracted from the images. Although it only represents a limited portion of the combustion chamber, the illuminated section of the jet should capture the important trends during the early phases of soot-formation. As the portion of the laser sheet containing LII signal is related to the volume of the soot cloud in the jet, the growth rate of the area containing LII signal is thus related to the early soot forming rate. The soot area is evaluated in a 90 degree

sector of the piston bowl with the jet in the middle. Signal levels above 2.5% of the dynamic range are considered to originate from soot. The area growth rate is evaluated as the slope of a linear curve fit to the soot areas during the first 5 CAD:s with LII signal. Figure 21 shows the soot area growth rate as function of O_2 mole fraction. The soot area growth rate increases rapidly as the O_2 fraction is decreased from 21% and peaks at 13% O_2. As the O_2 fraction is decreased further the soot area growth rate decreases again.

When comparing the trend in soot area growth rate with the trend in equivalence ratio at the lift-off position it might seem like they contradict each other. In the study about air entrainment the leanest conditions at the lift-off position appear at 14% O_2 fraction. This is thought to result in a relatively weak soot forming rate at this oxygen fraction. When looking at the same oxygen interval the soot area growth rate is the highest at 13% O_2 fraction, not far from where the weakest soot-formation would be expected in the air entrainment study. The measures are, however, related to different phases of the soot-formation. The equivalence ratio at the lift-off position gives information about the prerequisites for soot-formation during the quasi-steady jet-phase. Rich conditions combined with high combustion temperatures result in a large portion of fuel converting into soot. In contrast, the soot area growth rate is related to the transition between the premixed and mixing-controlled combustion phase.

During the premixed combustion phase all combustible fuel-air mixture burns off fast. However, if the mixture is rich, the premixed fuel will not be fully oxidized

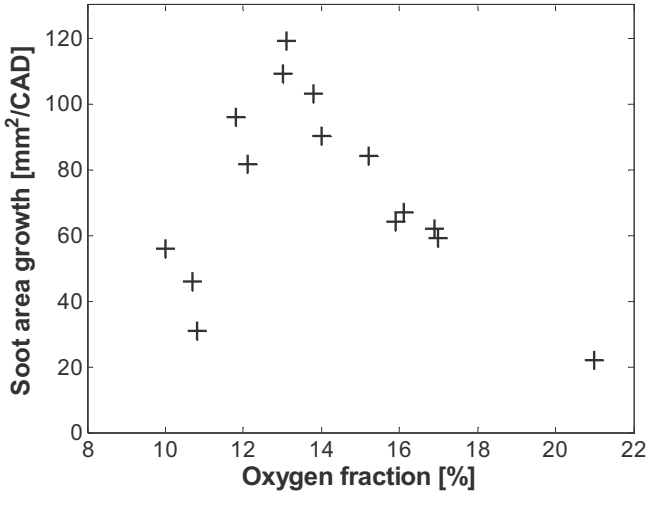

Figure 21 - Soot area growth rate during the first 5 images with LII-signal from 10 to 21% inlet O_2 mole fraction.

and if the equivalence ratio is above approximately 2 there will be soot in the combustion products [39]. It was indicated that a substantial part of the total fuel energy is trapped in partially oxidized fuel-rich mixtures after the premixed combustion phase. The soot area growth rate is related to the progression of the soot-formation in this fuel quantity. Furthermore, a fraction of the soot formed from this fuel quantity is likely to end up in the exhaust, especially during poor soot oxidation conditions. Note that both the trend in soot area growth rate and the trend in engine-out smoke in Fig. 17 peak in the middle of the O_2 fraction sweep.

One interesting observation presented in paper IV is that the position of the leading edge of the soot cloud is limited by soot oxidation above 16% O_2 fraction. Below 16% O_2 this measure is quite similar at a given time after SOI. The fact that this position is limited by soot oxidation is a strong indication of an effective soot oxidation during the steady-jet phase. If the position becomes stationary the fuel goes through all the steps of soot-formation and complete soot oxidation before the products leave the jet. In reality it is not evident that all soot is oxidized during this phase even if the downstream position of the jet becomes stationary since the jet characteristics might change towards end of injection. This explains, however, one observation from the air entrainment study. Recall that the engine-out soot was zero where the highest soot-formation was expected, as indicated by the red oval in Fig. 15. Since the oxygen fraction is 16% at this position it is right on the border where the leading edge of the soot is limited by soot oxidation in this study. It is thereby likely that a greater portion of the soot is oxidized during the quasi steady jet phase at this oxygen fraction compared with the rest of the test matrix. Also in the LII study the engine-out soot was zero above 16% O_2. This stresses the fact that a sufficient soot oxidation already during the jet phase is desirable. It also weights down the importance of the equivalence ratio at the lift-off position since it does not matter if the soot forming rate during the quasi-steady jet phase is high in cases where most of the soot is oxidized before the combustion products leave the jet.

To summarise: the equivalence ratio at the lift-off position showed a very low correlation to the engine-out soot. This indicates that the rate of soot-formation during the quasi-steady jet-phase is not dominant for the soot quantity that ends up in the exhaust despite the rather long injection duration used in the experiment. Since the trend in soot area growth rate shows a resemblance with the trend in engine-out smoke it is reasonable to assume that the soot-formation in the transition between the premixed and spray-driven combustion is of greater importance. Furthermore, it is indicated that factors creating good condition for soot-formation may favour a sufficient soot oxidation during the quasi-steady jet phase. The correlations to emissions of CO and UHC presented in Fig. 16 further

point to the importance of the oxidation process and the correlation to the heat release after EOI indicate that the late cycle oxidation is of importance.

The time resolved soot campaign was performed before the study about mechanical deformations (presented in section 4.1) and the heat release calculations did thereby not account for them. The heat release is thus re-evaluated in this thesis with respect to mechanical deformations. In paper IV two characteristics of the heat release, start of combustion and end of premixed combustion, was related to the start of soot-formation. Comparing Fig. 20 with Fig. 17 in paper IV it is seen that the evaluation of these quantities are not much affected by the mechanical deformation. The comparison between the heat release phases and start of soot-formation is thereby still valid with deformations.

In paper IV there is a discussion about the speed of the soot front. Even if this topic is not covered here a few sentences are spent on an error associated with Eq. 1 in the paper.

$$v = \frac{40.24}{t} \tag{30}$$

This equation describes the speed of the soot front in the plane of the laser sheet, v [mm/CAD], as function of t [CAD ASOI] in the interval between 4 and 22 CAD ASOI. The speed is estimated as the derivative of a logarithmic curve fit to the location of the soot front. In the paper manuscript it is, incorrectly, stated that the equation gives the jet speed as function of distance from the injector (Eq. 1 in the paper also uses x instead of t). The speed equation is given to provide a mathematical background to the residence time. However, in the analysis no actual speed is evaluated. The expression for the soot front position in mm from the injector,

$$S = 40.24 \cdot \ln(t) - 34.5 \tag{31}$$

is rewritten to extract the residence time in CAD,

$$t_{residence} = e^{(S_e+34.5)/40.24} - e^{(S_s+34.5)/40.24} \tag{32}$$

where S_e is the end position of the soot area and S_s is the start of the soot area. The evaluated residence time was thereby not affected by the error.

4.3 Sources of CO and UHC

Apart from soot and NO_x also CO and UHC are important for diesel engines, see Table 2 and 3. For low temperature combustion concepts these emissions can be harder to suppress below the legislation limit than NO_x and particulates. The

third part of this chapter focuses on the sources of CO and UHC. The baseline operating condition is at low load (3 bar $IMEP_g$) highly diluted (10% O_2) with early injection timing (-26.6 CAD ATDC). In the first subsection geometrical factors are varied to identify the main sources of CO and UHC for this base line condition. The second subsection contains a short discussion of how these sources are affected by the engine load, dilution level, and injection timing.

Influence of squish height and spray target

Earlier studies have observed not fully oxidized product in the squish volume after the main combustion event, for a low temperature combustion case [37,59]. To analyze the importance of this emission source, the present study investigates the distribution of CO and UHC in the clearance volume when geometrical factors are varied. The factors considered are the squish height and the spray target. Both the squish height and the spray target have a direct impact on the fuel-air mixing in the squish volume and are thereby important for the CO and UHC formation in this zone. Definitions of the squish height and spray target are given in Fig. 22. The squish height refers to the clearance between piston top and cylinder head. The spray target refers to the distance between piston top and the point where the spray axis intersects the piston lip (expressed in mm from baseline target). Both the squish height and the spray target are defined at TDC.

The specific engine-out emissions of CO and UHC are shown in Figs. 23 and 24, respectively. The trends in these emissions are quite similar: a larger squish height and smaller spray target value gives higher engine-out emissions.

A two photon excitation scheme for CO LIF was used with excitation in the deep UV, near 230.1 nm, and emission between 440 and 730 nm. The excitation wavelength also promotes C_2 fluorescence, emitting between 420 and 520 nm. The C_2 fluorescence is expected to arise from laser-induced fragmentation fluorescence

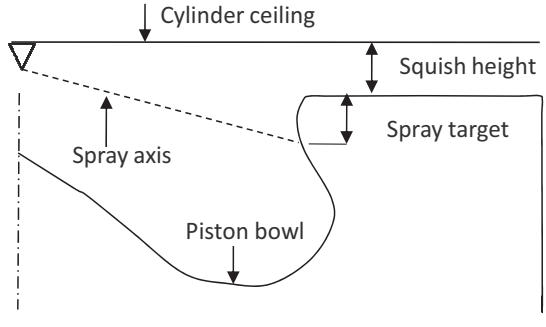

Figure 22 - Definitions of spray target and squish height. It should be noted that the spray target is a function of both injector tip protrusion and squish height. When increasing the squish height the injector tip protrusion must therefore increase to maintain a constant spray target. A larger spray target value corresponds to aiming lower on the piston lip.

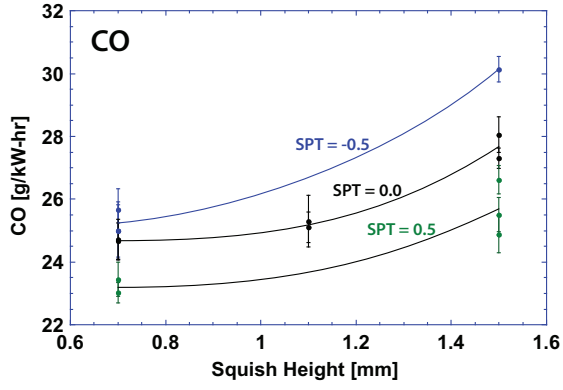

Figure 23 - Engine-out emissions of CO as function of squish height for three different spray targets (expressed in mm from baseline target).

(LIFF) of acetylene (C_2H_2), the vinyl radical (C_2H_3), or butadiene (C_4H_6) among other possible UHC species [60]. Each of these species is a combustion intermediate present in the combustion of both lean and rich mixtures. C_2H_2 is not only an intermediate species as it is expected also in the product gases of rich mixtures. Finally fluorescence from PAH, including smaller PAH that absorb more at shorter wavelengths, were excited. The PAH fluorescence is indicative of either largely unreacted parent fuel or of hot products of rich ($\Phi > 2$) combustion.

The optical data consist of spectrally resolved measurements along a radius at different heights in the clearance volume. The radius between 0 and 40 mm from the cylinder centerline is divided in 24 equally long sections (1.67 mm long each). At 50 CAD ATDC measurements were performed at three heights. As discussed above, UHC are measured as both PAH and C_2. Figure 25 shows the mean

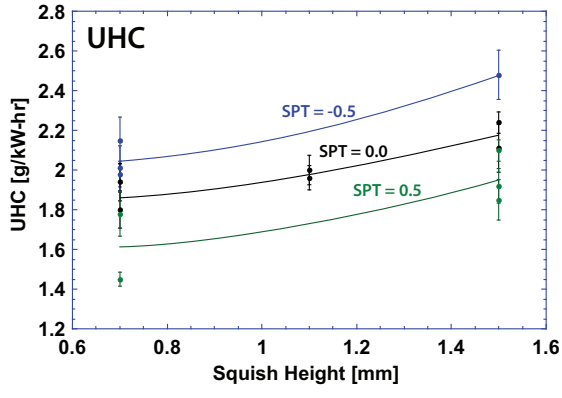

Figure 24 - Engine-out emissions of UHC as function of squish height for three different spray targets (expressed in mm from baseline target).

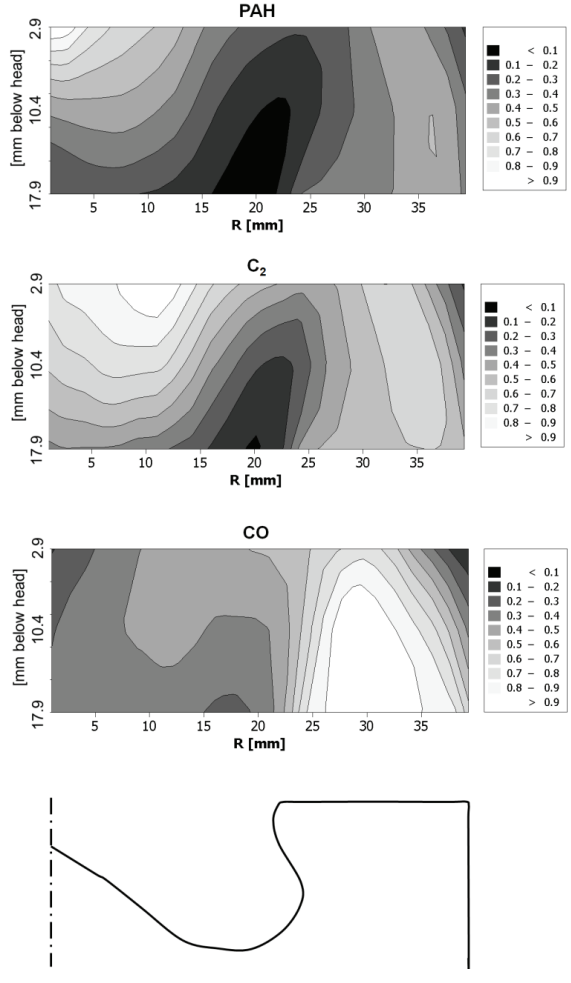

Figure 25 - Spatial distribution of PAH, C_2, and CO in the clearance volume 50 CAD ATDC. The contours are generated by averaging all measurements in the test matrix.

distributions of PAH, C_2, and CO at 50 CAD ATDC. The contour plots are generated by averaging 14 replicates with 50 cycles in each replicate i.e. totally 700 fired engine cycles and should thus give a good picture of the mean distribution.

Although UHC and CO emissions near the injector and cylinder centerline are not a central focus of this work, some discussion is merited as large concentrations of UHC are observed in this region. Recall that the PAH signal is anticipated to arise from both the parent fuel compounds and very rich regions, while C_2 arises from combustion intermediates and products of fuel rich combustion.

Thus, the observation at 50 CAD of higher levels of PAH near the injector with C_2 peaking further away is consistent with two possible situations: 1) the presence of largely unburned fuel near the injector, which has undergone progressively more oxidation as radial distance from the injector increases, and 2) very rich, burned mixture near the injector, becoming progressively leaner as radial distance increases. In the first case, high PAH concentration close to the injector could be related to injector fuel dribble and/or to lean mixtures of unreacted fuel formed during the closing flank of the injection rate profile [60,61]. In the second case, only injector dribble would likely contribute to the observed PAH.

Measurements are not made within the bowl. However, velocity measurements performed at the baseline condition [62] show that bulk-gases escape the bowl during the expansion stroke and enter the central region of the clearance volume just inside of the bowl lip radius. Within this region, the measurements indicate very little CO, PAH or C_2 at 50 CAD. In fact, concentrations of these species appear to be at a minimum in this region. Accordingly, only a small fraction of the engine-out CO and UHC emissions stem from the bowl, and the deterioration in combustion efficiency and emissions observed in Figs. 23–24 is not likely to be caused by changes in the emissions from this region.

In contrast to this, Fig. 25 shows concentrations of PAH and C_2 in the squish volume that are nearly as great as those observed near the injector. The observed PAH is concentrated along the cylinder sidewall, while peak amounts of C_2 are observed slightly away from the wall. Peak CO is concentrated even further towards the centerline, before decreasing rapidly near the bowl lip. These observations are consistent with a gradient in "reactedness", potentially controlled by thermal variations within the squish volume. Near the cylinder wall, where temperatures are expected to be the coolest, fuel oxidation proceeds very slowly—resulting in lower levels of combustion intermediates and almost no CO, which is only present at the later stages of combustion. Moving inwards towards the cylinder centerline, the degree of reaction progressively increases, resulting in increased CO. Finally, approaching the bowl lip, the combustion temperatures are sufficient to oxidize CO as well.

The CO and UHC emissions are significantly impacted, if not dominated, by mixture in the squish volume. Changes observed in engine-out emissions as squish height and spray targeting are varied can accordingly be attributed to changes in the emissions emanating from this region.

The data was further analyzed by comparing the relative portion of signal occurring in different zones. Such a comparison can accentuate areas that are of importance for the engine-out emissions. The analysis strengthened the indication that the squish volume is important for the engine-out CO and UHC.

The left part of Fig. 26 shows the portion of signal occurring in the upper corner of the squish volume as function of spray target and squish height. The level corresponds to the signal in the squish zone of the measurement closest to the head divided by the total signal in all three measurements. This is illustrated by

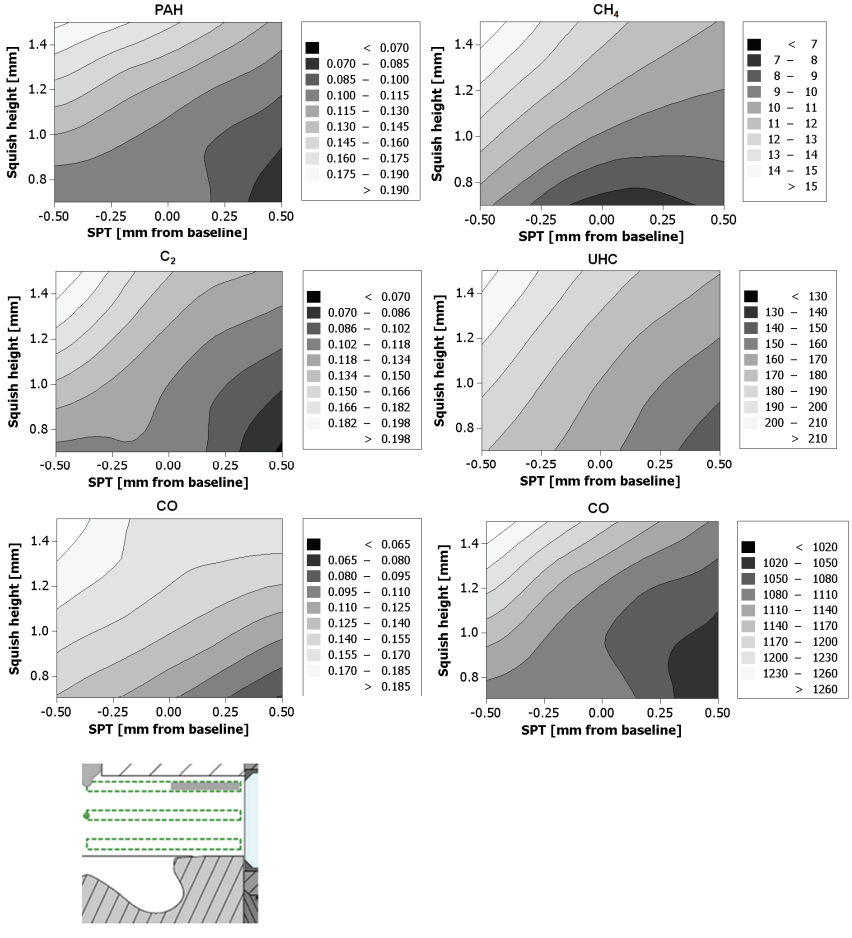

Figure 26 - The left column shows the relative portion of the total signal in the upper part of the squish zone 50 CAD ATDC for PAH, C_2 and CO (the signal inside the gray square divided with the signal inside the dashed squares). The right column shows the engine-out emissions in ppm. The engine is only fired every fifth cycle and the emission concentrations in the exhaust are thereby lower than for a continuously fired engine. Both columns are expressed as function of squish height and spray target.

the small image in the bottom of Fig. 26. The right part of Fig. 26 shows the engine-out emissions of CH_4, total UHC, and CO as function of squish height and spray targeting. The close agreement between the trends in the right and left part of Fig. 26 indicates that the upper squish volume is an important zone for the trends in engine-out emissions.

The trends for the different engine-out emissions are quite similar: a larger squish height and smaller spray target value gives higher engine-out emissions. The absolute levels of CH_4 in Fig. 26 are typically only 5–7% of the total UHC. More CH_4 is expected to be produced in rich zones than in lean [54]. Hence, this indicates that the bulk of the UHC emissions are likely to originate from overly lean regions.

This study shows that the squish volume is an important zone for CO and UHC emissions control in the studied low temperature combustion case and that the major contribution is coming from overly lean zones. A small squish volume and a large spray target, i.e. aiming low on the piston, produces lower engine-out emissions. In the attempt to achieve clean LTC it is essential to place a minimum amount of fuel in the squish volume.

This investigation was performed before the investigation about mechanical deformation (presented in section 4.1). In paper III some conclusions are drawn from the trends in premixed burn time as function of squish height and spray target. However, since the whole test matrix uses the same load, TDC pressure, and essentially the same combustion phasing the trends in heat release calculations is not expected to be affected if the deformation were considered.

Impact of load, dilution, and injection timing

The deep UV LIF technique described above was later used in papers VII and VIII. In paper VII the impact of engine load and dilution level were investigated at the baseline operating condition (3 bar $IMEP_g$ and 10% O_2). Paper VIII studied the baseline load but used a late injection strategy, near TDC, and a less diluted condition (15% O_2 mole fraction).

The engine-out emissions of CO and UHC decreased with increasing load and O_2 fraction. Also the LIF images indicated a drastic decrease in CO concentration during these conditions but the peak signal levels were found in the squish volume independently of load and O_2 fraction. C_2 and PAH show similar trends with engine load and dilution level as CO does. However, as in the previous study, in addition to the squish volume, also the region close to the injector was an important source of these emissions.

The late injection combustion case in paper VIII with SOI at -2.3 CAD ATDC showed increased engine-out levels of UHC but decreased CO levels compared to

the baseline. The combustion efficiency was 97% compared to 98% for the baseline. When the injection was retarded even further to -0.5 CAD ATDC the emissions increased drastically and the combustion efficiency was 95%.

Figure 27 shows the CO distribution 50 CAD ATDC for the late injection cases. The left plot with SOI at -2.3 CAD ATDC shows a quite distributed CO signal. The signal levels peak close to the ceiling in the squish volume. When the injection is further retarded to -0.5 CAD ATDC the signal levels in the squish volume clearly dominate the rest of the clearance volume. The drastic increase in engine-out levels of CO and UHC are expected to arise from this zone. The distribution of UHC is not shown but is quite similar as for CO except that more signal from the central clearance volume is evident for the case with SOI at -0.5 CAD ATDC. Since the injection occurs when the piston top is close to TDC little fuel is expected to be placed in the squish volume during the injection event. However, it was shown that fuel accumulated on the bowl-pip during high-temperature heat release was transported into the squish-volume by the reverse squish flow. Squish volume CO and UHC are expected to mainly arise from this fuel quantity.

In summary: the experimental results in both studies indicated that the squish volume still was the major source of CO and a significant source of UHC when the load, dilution level, and injection timing were changed. This makes the conclusion from the previous study more general.

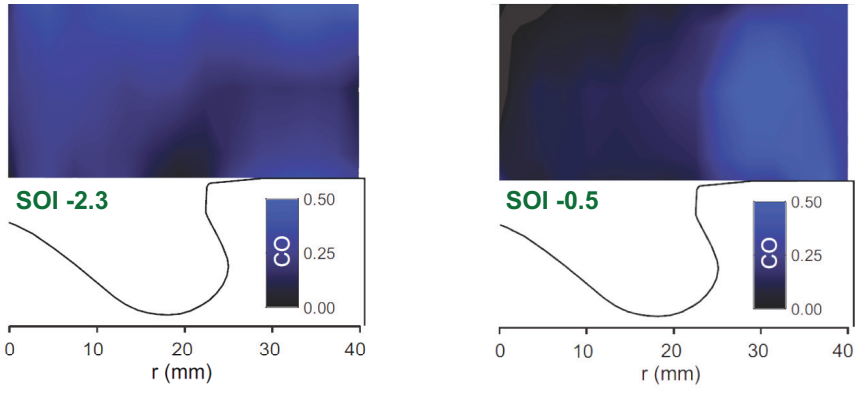

Figure 27 - Distribution of CO 50 CAD ATDC for the baseline load 3 bar $IMEP_g$. The O_2 mole fraction is 15% and the start of injection timing in CAD ATDC is indicated in the images.

Chapter 5

Concluding remarks

This chapter contains a brief summary of the main observations and contributions of the work in this thesis. The limitations and possible extensions of the studies performed are also discussed.

5.1 Evaluation of optical engines

Mechanical deformation

The studies about mechanical deformation revealed that the distortions of the in-cylinder volume trace due to mechanical deformation causes errors in heat release calculations. It was shown that an adjustment of the compression ratio cannot compensate for these deformations. However, the usage of deformation constants and/or motored heat release subtraction did reduce the errors in heat release calculation significantly. The focus of the studies was to investigate the impact of deformations on optical engines but since it was indicated that a significant portion of the total deformations came from the all-metal engine parts these engines were included in the analysis. The largest impact came from compression of the moving parts i.e. crank axis, connecting rod, piston, and piston extension due to gas-forces. About half of the deformations of the moving parts were associated with the all-metal engine, see paper VI.

If the deformations need to be considered or not depends on three things: the stiffness of the engine, the load case, and what the heat release analysis should be used for. If high peak cylinder pressures or steep pressure gradients are used in optical engines the shape of the rate of heat release will be largely distorted. Evaluation of quantitative information, for example crank angle degree of 90% heat release completion or portion of premixed heat release, are likely to give false information. If such information is essential it is also essential to consider the deformations. In some cases even a qualitative evaluation of the rate of heat release shape might lead to false conclusions. In contrast, low and moderate peak cylinder pressures and pressure gradients on all-metal engines do not affect the heat release calculation substantially. To justify the efforts to account for pressure deformations in all-metal engines, the load case must be stressful or the

aim must be to accurately extract quantitative information from the heat release analysis. It is also important to point out that even if the deformations are considered, there is no guarantee that the calculated rate of heat release is accurate since there are still other uncertainties such as mass and heat losses. It might, however, be more straightforward to consider these uncertainties when the in-cylinder volume trace is accurately determined.

The dynamic aspects of the deformations due to steep pressure gradients are not yet analyzed in this thesis. The deformations presented are measured during motored operation but the same equations are used to handle fired pressure traces. The possible issue with this is that it is not evident that the dynamic behaviour is the same for the two cases. During motored operation the pressure derivatives are much smaller than during fired operation, especially in the vicinity of TDC. The dynamic aspects of mechanical systems such as an engine can be modelled by a spring and a damper. The movement, x, of the mass, m, due to an applied force, F, is given by

$$F = kx + c\frac{dx}{dt} + m\frac{d^2x}{dt^2} \tag{33}$$

In the studies of paper V and VI the damping constant, c, was set to zero and the acceleration term was ignored. Only the spring constant part, kx, was included. The errors from this simplification will now be tested. The deformation,

$$x = \frac{A \cdot p(\vartheta)}{k} \tag{34}$$

is calculated for the evaluated case with the steepest pressure gradient. In Eq. 34 A is the cylinder cross section area, and p is the cylinder pressure as function of CAD, ϑ. The magnitudes of the second and third terms of Eq. 33 are calculated with the first and second derivative of x from Eq. 34. Note that these terms have nothing to do with the crank driven piston movement. It is only the very small movement due to the pressure gradient that is considered here. The whole mass of the moving parts is used as m and the damping constant, c, is calculated from the damping ratio of aluminium according to [63]. The terms from the first and second order derivative of x turn out to be small compared to the kx term - at maximum 0.5% - when the signals are low pass filtered with a cut-off frequency of 0.63 CAD^{-1}. Accordingly the simplification of Eq. 33 does not lead to any significant errors.

One related topic that would be interesting to investigate is how the distorted volume trace affects engine simulations. In three dimensional computational fluid dynamics models the mesh grid is designed to closely follow the in-cylinder

volume as function of CAD. If the distortion is not considered the mesh will not describe the reality and the calculated flows are likely to be affected. It is hard to predict the impact of a distorted mesh but it would be interesting to analyze.

Effects of the optical access

It was shown that it is possible to achieve realistic engine-out emissions from an optical engine configuration by adjusting the charge temperature until the combustion phasing was similar to a metal engine configuration. If a specific operation condition from an all-metal engine is investigated on an optical engine, it is thereby a good approach to match the rate of heat release between the engines.

The observed differences in the study were all related to lower heat conductivity of quartz compared to aluminium and steel. This implies that the effect on the combustion process will be larger the closer to the wall the combustion occurs. A classic diesel combustion case with a large portion of spray-driven combustion will probably be less affected than a combustion case with a large portion of premixed combustion. This was partly verified when two configurations with different piston bowl material were compared over a variety of inlet temperatures. When the configurations were operated at an inlet temperature of 388 K the differences were smaller than when the inlet temperature was 358 K. A decreased inlet temperature extends the ignition delay and produces a greater premixed portion of the heat release. This is something that would be interesting to further investigate.

The combustion case in the second part of chapter 4 where soot processes are studied has a rather large portion of spray-driven combustion. The combustion should therefore be less affected by the optical access than a combustion case with a large portion of premixed combustion, according to the discussion above. The focus of the presented investigations is to extract trends rather than quantitative information so the conclusions are thus not likely to be limited by the optical access.

The study in the third part of chapter 4 where sources of CO and UHC are investigated are at greater risk to be affected by the optical access. The comparison between optical and all-metal engines shows that the higher surface temperature of optical parts lowers the engine-out emissions of incompletely oxidized products. The studied combustion case is furthermore a partially premixed LTC concept with a large portion of the combustion close to the walls, which probably is more affected by the optical access. However, this is the same engine that is used in [5] where it was verified that realistic trends in engine-out emissions were achieved. The knowledge from [5] is used in this campaign to obtain a consistent thermal state of the engine by following a strict operating

schedule. Finally, also here the main focus was on the trends and the main conclusions will still be valid even if the surface temperature would differ slightly.

5.2 Soot processes

The work about soot processes focuses on the relation between jet-characteristics and engine-out soot emissions. It is indicated that a substantial portion of the fuel energy is left in fuel-rich mixtures that are not completely oxidized after the premixed combustion phase. The soot area growth rate in the jet that is thought to be coupled to this fuel quantity shows resemblances with the trend in engine-out smoke over a sweep in inlet O_2 mole fraction. The trends in air entrainment up to the lift-off position, on the other hand, show a very weak correlation with the engine-out soot. The soot area growth rate is related to the transition between the premixed and the spray-driven combustion phase. In contrast, the equivalence ratio at the lift-off position is thought to be important for the soot forming rate during the quasi-steady jet-phase. This indicates that the rate of soot-formation during the quasi-steady jet-phase has a rather weak relation to the level of engine-out soot. This is despite the usage of few, small, nozzle holes leading to a long injection duration with a large portion of the combustion taking place during the fuel injection period. The observation is explained as follows: first, a large fraction of the soot is formed in the transition between the premixed and spray-driven combustion which weighs down the importance of the quasi-steady jet-phase. Second, factors that enhance the soot formation during the quasi-steady jet-phase in some cases also enhances the soot oxidation during this phase. Third, correlations to emissions of CO and UHC further point to the importance of the oxidation process and characteristics of the heat release indicates that this is partly related to the late cycle.

A natural continuation of the work about soot processes would be to investigate the late cycle soot oxidation. One interesting approach would be to measure this by the laser extinction method vertically through the combustion chamber during the expansion. The laser extinction is related to the absorption and scattering by soot aerosols [64]. This could be done fairly simply with a laser sent through an optical fibre in the cylinder head with collection on a fast photo diode via the mirror in the bottom of the piston extension. If the engine is operated in skip fire mode the attenuation during the motored cycles can be used as a zero reference. Since the extinction is measured vertically the same portion of the in-cylinder volume will be analyzed independently of the piston position. If the whole expansion stroke is monitored it would be possible to quantify the decrease in attenuation which is directly related to the soot oxidation. Since the soot distribution is inhomogeneous and essentially stochastic this would require averaging over a large number of cycles and/or the usage of several optical fibres.

5.3 Sources of CO and UHC

The studies about sources of CO and UHC show that the squish volume is a major contributor to the engine-out emissions. The baseline operating condition uses an early injection timing, -26.6 CAD ATDC, and a greater portion of the fuel is placed in the squish volume the earlier the fuel is injected. The combustion case in paper VIII uses an injection timing near TDC but the squish volume is still indentified as the major source of CO and an important source of UHC. Since two combustion concepts with such different injection strategies point out the squish volume as the major source of not fully oxidized products it shows that the importance of this source is not easily erased.

The studies raise the question if low temperature combustion systems would benefit from completely new hardware. The combustion chamber design is strongly connected to the combustion mode [65]. It is therefore not advisable to take a combustion chamber that is optimized for one combustion mode and use it for another. The investigation showed that the reactions progress slower in the squish volume and it is thereby important to minimize the fuel placed in this region. For the case with early injection this can be achieved with a smaller included angle of the sprays. It might however be beneficial to minimize the squish volume itself. A shallow, wide bowl with a small squish area gives a smaller squish volume. Such a piston bowl would be interesting to investigate together with a fuel injector with a smaller included angle. However, some combustion concepts are meant to use LTC at low load and conventional diesel combustion at high load. In these cases it will be hard to find an optimum piston bowl design.

References

[1] Cummins, C.L. Jr, Internal Fire, dba Carnot Press, Wilsonville, OR, 2000

[2] Statistics over the usage of diesel engine powered vehicles, available at: http://www.acea.be, 17/2/2011

[3] Foyt, G., Demonstration and evaluation of Hybrid Diesel-Electric Transit Buses-Final Report, Connecticut Academy of Science and Engineering R, CT-170-1884-F-05-10, 2005

[4] Trajkovic, S., Tunestål, P., and Johansson, B., A Simulation Study Quantifying the Effects of Drive Cycle Characteristics on the Performance of a Pneumatic Hybrid Bus, ASME Technical Paper ICEF2010-3509, 2010

[5] Colban, W.F., Kim, D., Miles, P.C., Oh, S., Opat, R., Kreiger, R., Foster, D., Durrett, R.P., and Gonzalez D.M.A., A Detailed Comparison of emissions and Combustion Performance between Optical and Metal Single-Cylinder Diesel Engines at Low Temperature Combustion Conditions, SAE Technical Paper 2008-01-1066, 2008

[6] Aronsson, U., Chartier, C., Horn, U., Andersson, Ö., Johansson, B., and Egnell, R., Heat Release Comparison Between Optical and All-Metal HSDI Diesel Engines, SAE Technical Paper 2008-01-1062, 2008

[7] Griffiths, J.F. and Barnard, J.A., Flame and Combustion 3rd Ed., Alden press, Oxford, 1995

[8] Eckbreth, A.C., Laser Diagnostics for combustion temperature and species, Second edition, Gordon and Breach Publishers, Amsterdam, 1996

[9] Encyclopaedia of Laser Physics and Technology, available at http://www.rp-photonics.com/q_factor.html 7/3 /2011

[10] Svelto, O., Principles of Lasers, 3rd Ed., Plenum press, New York, 1989

[11] Lang, O.R., Triebwerke schnellaufender verbrennungsmotoren grundlagen zur berechnung und konstruktion, Springer-Verlag, Berlin, 1966

[12] Heywood, J.B., Internal Combustion Engine Fundamentals, McGraw-Hill Book Co, New York, NY, 1988

[13] Johansson, B., Förbränningsmotorer, Division of combustion engines, LTH, Lund, 2006

[14] Woschni, G., A Universally Applicable Equation for the Instantaneous Heat Transfer Coefficients in the Internal Combustion Engine, SAE Technical Paper 670931, 1967

[15] Tunestål, P., Self-tuning gross heat release computation for internal combustion engines, Control Engineering Practice 17 518–524, 2009

[16] Young, D.F., Munson, B.R., and Okiishi, T.H., A Brief Introduction to Fluid Mechanics, John Wiley & Sons, Inc., Hoboken, NJ, 2004

[17] Cengel, Y.A. and Boles, M.A., Thermodynamics: An engineering approach, 4th Ed., McGraw-Hill Book Co, New York, NY, 2002

[18] Miles, P.C., Choi, D., Pickett, L.M., Singh, I.P., Henein, N., Rempelewert, B.H., Yun, H., and Reitz, R.D., Rate-Limiting Processes in Late-Injection Low-Temperature Diesel Combustion Regimes, Thiesel, Valencia, Spain, 2004

[19] Egnell, R., Combustion Diagnostics by means of Multizone Heat Release Analysis an NO Calculation, SAE Technical Paper 981424, 1998

[20] Weiss, M.A., Data structures & Problem Solving using JAVA, Addison Wesley Inc., Reading, MA, 2001

[21] JAVA programming language. Available at: http://www.oracle.com/technetwork/java/index.html 12/3 2011

[22] Emission standards. Available at: http://www.dieselnet.com/standards 1/3 2011

[23] Stone, R., Introduction to Internal Combustion Engines, Antony Rowe Ltd, Chippenham, 1999

[24] Christian, R., Knopf, F., Jaschek, A., and Schindler, W., Eine Neue Messmethodik der Bosch-Zahl mit Erhöhter Empfindlichkeit, Motortech. Z., 54:16–22, 1993

[25] Diesel-Engine Management 2nd Ed., Bosch, Robert GmbH, Stutgart, 1999

[26] Emissions Measurement procedure. Available at: http://www.epa.gov/ttn/emc, 25/3 2011

[27] Siebers, D.L., Scaling Liquid-Phase Fuel Penetration in Diesel Sprays Based on Mixing-Limited Vaporization, SAE Technical Paper 1999-01-0528, 1999

[28] Information about Scania XPI injection system. Available at: http://scaeuro5.stage5.leon.se/com/en/Inline/technology/xpi 1/3 2011

[29] Jääskelläinen, H., Low Temperature Combustion, Available at: www.dieselnet.com, 12/3 2011

[30] Kimura, S., Aoki, O., Ogawa, H., Muranaka, S., and Enomoto, Y., New Combustion Concept for Ultra Clean and High Efficiency Small DI Diesel Engines, SAE Technical Paper 1999-01-3681, 1999

[31] Kimura, S., Aoki, O., Kitahara, Y., and Aiyoshizawa, E., Ultra clean Combustion Technology Combining a Low-Temperature and Premixed Combustion Concept for Meeting Future Emission Standards, SAE Technical Paper 2001-01-0200, 2001

[32] Yanagihara, H., Ignition Timing Control At Toyota "UNIBUS", Combustion System, chapter in A New Generation of Engine Combustion Processes for the Future?, OP. Ed. Duret P., Editons Technip, Paris, 2001

[33] Noehre, C., Andersson, M., Johansson, B., and Hultquist, A., Characterization of Partially Premixed Combustion, SAE Technical Paper 2006-01-3412, 2006

[34] Lewander, C.M., Ekholm, K., Johansson, B., Tunestål, P., Keeler, N., Milovanovic, N., Harcombe, T., and Bergstrand, P., Investigation of the Combustion Characteristics with Focus on Partially Premixed Combustion in a Heavy Duty Engine, SAE Technical Paper 2008-01-1658, 2008

[35] Okude, K., Mori, K., Shiino, S., and Moriya, T., Premixed Compression Ignition (PCI) Combustion for Simultaneous Reduction of NO_x and Soot in Diesel Engines, SAE Technical Paper 2004-01-1907, 2004

[36] Lechner, C.A., Jacobs, T., Chryssakis, C., Assanis, D.N., and Siewert, R.M., Evaluation of a Narrow Spray Cone Angle, Advanced Injection Timing Strategy

to Achieve Partially Premixed Compression Ignition Combustion in a Diesel Engine, SAE Technical Paper 2005-01-0167, 2005

[37] Kim, D., Ekoto, I., Colban, W.F., and Miles, P.C., In-Cylinder CO and UHC Imaging in a Light-Duty Diesel Engine During PPCI Low-Temperature Combustion, SAE Technical Paper 2008-01-1602, 2008

[38] Dec, J.E., A Conceptual Model of DI Diesel Combustion Based on Laser-Sheet Imaging, SAE Technical Paper 970873, 1997

[39] Akihama, K., Takatori, Y., Inagaki, K., Sasaki, S., and Dean, A.M., Mechanism of the Smokeless Rich Diesel Combustion by Reducing Temperature, SAE Technical Paper 2001-01-0655, 2001

[40] Svensson, K.I., Effects of Fuel Molecular Structure and Composition on Soot Formation in Direct-Injection Spray Flames, Dissertation, Brigham Young University, 2005

[41] Naber, J.D. and Siebers, D.L., Effects of Gas Density and Vaporization on Penetration and Dispersion of Diesel Sprays, SAE Technical Paper 960034, 1996

[42] Pickett, L.M., Siebers, D.L., and Idicheria, C.A., Relationship Between Ignition Processes and the Lift-Off Length of Diesel Fuel Jets, SAE Technical Paper 2005-01-3843, 2005

[43] Idicheria, C.A. and Pickett, L.M., Effect of EGR on Diesel Premixed-Burn Equivalence Ratio, Proceedings of the Combustion Institute, 31:2931-2938, 2007

[44] Idicheria, C.A. and Pickett, L.M., Soot Formation in Diesel Combustion under High-EGR Conditions, SAE Technical Paper 2005-01-3834, 2005

[45] Idicheria, C.A. and Pickett, L.M., Effects of Ambient Temperature and Density on Soot Formation under High-EGR Conditions, Thiesel, Valencia, Spain, 2006

[46] Pickett, L.M. and Siebers, D.L., Non-Sooting, Low Flame-Temperature Mixing-Controlled DI Diesel Combustion, SAE Technical Paper 2004-01-1399, 2004

[47] Picket, L.M. and Siebers, D.L., Soot Formation in Diesel Fuel Jets Near the Lift-Off Length., International Journal of Engine Research, 7:349-370, 2006

[48] Musculus, M.P.B., Multiple Simultaneous Optical Diagnostic Imaging of Early-Injection Low-Temperature Combustion in a Heavy-Duty Diesel Engine, SAE Technical Paper 2006-01-0079, 2006

[49] Musculus, M.P.B., Effects of the In-Cylinder Environment on Diffusion Flame Lift-Off in a DI Diesel Engine, SAE Technical Paper 2003-01-0074, 2003

[50] Aronsson, U., Chartier, C., Andersson, Ö., Egnell, R., Sjöholm, J., Richter, M., and Aldén, M., Analysis of the Correlation Between Engine-Out Particulates and Local Φ in the Lift-Off Region of a Heavy Duty Diesel Engine Using Raman Spectroscopy, SAE Technical Paper 2009-01-1357, 2009

[51] Van Basshuysen, R. and Schäfer, F., Internal Combustion Engine Handbook, SAE International, 2004

[52] Upatnieks, A., Mueller C.J., and Martin G.C., The Influence of Charge-Gas Dilution and Temperature on DI Diesel Combustion Processes Using a Short-Ignition-Delay, Oxygenated Fuel, SAE Technical Paper 2005-01-2088, 2005

[53] Koci, C.P., Ra, Y., Krieger, P., Adrie, M., and Foster, D.E., Detailed Unburned Hydrocarbon Investigations in a Highly Dilute Diesel Low Temperature Combustion Regime, SAE Technical Paper 2009-01-0928, 2009

[54] Cook, D.J., Pitsch, H., and Nentwig, G., Numerical Investigation of Unburnt Hydrocarbon Emissions in a Homogeneous-Charge Late-Injection Diesel-Fueled Engine, SAE Technical Paper 2008-01-1666, 2008

[55] Opat, R., Ra, Y., Gonzales D.M.A., Krieger, R., Reitz, R.D., Foster, D.E., Durett, R.P., and Siewert, R.M., Investigation of Mixing and Temperature Effects on HC/CO Emissions for Highly Dilute Low Temperature Combustion in a Light Duty Diesel Engine, SAE Technical Paper 2007-01-0193, 2007

[56] Kashdan, J.T., Mendez, S., and Bruneaux, G., On the origin of Unburned Hydrocarbon Emissions in a Wall Guided, Low NO_x Diesel Combustion System, SAE Technical Paper 2007-01-1836, 2007

[57] Lide, D.R., Handbook of Chemistry and Physics, CRC Press LLC, Boca Raton, FL, 2000

[58] Freund, J., E., Perles, B., M., Modern Elementary Statistics, Pearson Prentice Hall, Upper Saddle River, NJ, 2007

[59] Ekoto, I., Colban, W.F., Miles, P.C., Wook Park, S., Foster, D.E., and Reitz, R.D., UHC Emissions Sources from a Light-Duty Diesel Engine Undergoing Dilution Controlled Low Temperature Combustion, SAE Technical Paper 2009-01-1446, 2009

[60] Osborn, D. L. and Frank, J. L., Laser-induced fragmentation fluorescence detection of the vinyl radical and acetylene, Chemical Physics Letters, 349:43-50, 2001

[61] Musculus, M. P. B., Lachaux, T., Pickett, L. M., and Idicheria, C. A., End-of-Injection Over-Mixing and Unburned Hydrocarbon Emissions in Low-Temperature-Combustion Diesel Engines, SAE Technical Paper 2007-01-0907, 2007

[62] Colban, W. F., Ekoto, I. W., Kim, D., and Miles, P. C., In-Cylinder Velocity Measurements in an Optical Light-Duty Diesel at LTC Conditions, Thiesel, Valencia, Spain, 2008

[63] Adams, V. and Askenazi A., Building Better Products with Finite Element Analysis, OnWord Press, Santa Fe, N.M., 1999

[64] Musculus, M.P., Picket, L.M., Diagnostic considerations for optical laser-extinction measurements of soot in high-pressure transient combustion environments, Combustion and Flame 141:371–391, 2005

[65] Andersson, Ö., Diesel Combustion, in Handbook on Combustion, vol. 3, Ed. Winter F., Wiley-VHC books, Weinheim, 2010

Summary of papers

7.1 Paper I

Heat Release Comparison Between Optical and All-Metal HSDI Diesel Engines

Ulf Aronsson, Clément Chartier, Uwe Horn, Öivind Andersson, Bengt Johansson, Rolf Egnell

Division of Combustion Engines, Lund University, Sweden

SAE Technical paper 2008-01-1062

The impact of the modifications needed to achieve optical access on the combustion and engine-out emissions was investigated. The analysis showed that there were differences in both combustion phasing and engine-out emissions if the engines were operated in the same manner. All differences were related to the lower heat conductivity of quartz compared to aluminum and steel. Fortunately, it was possible to compensate for the observed differences by lowering the inlet temperature in the optical engine configuration.

Experiments were performed together with Clément Chartier and Uwe Horn. I post-processed the data and took the main responsibility of the paper writing which was carried out together with Öivind Andersson.

7.2 Paper II

Analysis of the Correlation Between Engine-Out Particulates and Local Φ in the Lift-Off Region of a Heavy Duty Diesel Engine Using Raman Spectroscopy

Ulf Aronsson[1], Clément Chartier[1], Öivind Andersson[1], Rolf Egnell[1]
Johan Sjöholm[2], Mattias Richter[2], Marcus Aldén[2],

[1]Division of Combustion Engines, Lund University, Sweden
[2]Division of Combustion Physics, Lund University, Sweden

SAE Int. J. Fuels Lubr. October 2009 2:645-660/2009-01-1357

In this paper a correlation analysis between the engine-out soot particulates and factors related to the soot forming process was performed. The local equivalence ratio, Φ, at the lift-off position was chosen as the main measure related to the soot forming process. Φ was measured in the interior of the jet using Raman spectroscopy and scaled to the lift-off position using a well established expression of the air entrainment in diesel jets. The correlation analysis showed a surprisingly low correlation between the factors related to the soot forming

process and the engine-out soot particulates. Factors related to the soot oxidation process showed on the other hand a much stronger correlation.

Experiments were performed together with Johan Sjöholm and Clemént Chartier. Johan Sjöholm and I post-processed the data. I took the main responsibility of the paper writing which was carried out together with Johan Sjöholm and Öivind Andersson. The authors from the Division of Combustion Engines were the main responsible for the engine while the authors from the Division of Combustion Physics were the main responsible for the laser technique.

7.3 Paper III

Influence of Spray-Target and Squish Height on Sources of CO and UHC in a HSDI diesel engine during PPCI Low-Temperature Combustion

Ulf Aronsson[1], Öivind Andersson[1], Rolf Egnell[1]
Paul C. Miles[2,1] , Isaac W. Ekoto[2]

[1]Division of Combustion Engines, Lund University, Sweden
[2]Sandia National Laboratories, Livermore, CA, United States

SAE Technical paper 2009-01-2810

The impact of geometrical factors on the relation between the in-cylinder distribution and the engine-out emissions of CO and UHC was investigated. Laser induced fluorescence, LIF, near 230.1 nm was used to excite CO and UHC in the clearance volume during low temperature combustion. The geometrical factors considered were the squish height and the spray targeting on the piston. A large squish height and a spray target high on the piston gave elevated engine-out CO and UHC emissions. This was related to the relative distribution in the clearance volume of these emissions. It was concluded that the fuel placed in the squish volume during the injection event is closely related to the engine-out emissions.

Experiments were performed together with Paul Miles. I took the main responsibility of the paper writing which was carried out together with Paul Miles. Paul Miles was the main responsible for the laser technique.

7.4 Paper IV

Analysis of EGR Effects on the Soot Distribution in a Heavy Duty Diesel Engine using Time-Resolved Laser Induced Incandescence

Ulf Aronsson[1], Clément Chartier[1], Öivind Andersson[1], Bengt Johansson[1]
Johan Sjöholm[2], Rikard Wellander[2], Mattias Richter[2], Marcus Aldén[2]
Paul C. Miles[3,1]

[1]Division of Combustion Engines, Lund University, Sweden
[2]Division of Combustion Physics, Lund University, Sweden
[3]Sandia National Laboratories, Livermore, CA, United States

SAE Int. J. Engines December 2010 3:137-155 /2010-01-2104

In this paper the soot distribution as function of ambient O_2 mole fraction in a heavy-duty diesel engine was investigated at low load (6 bar $IMEP_g$) with time resolved laser induced incandescence (LII). It is well known that the engine-out smoke level increases with decreasing O_2 fraction up to a certain level where it starts to decrease again. For the studied case the peak occurred at an O_2 fraction of 11.4%. The initial growth rate of the soot area, in the plane of the laser sheet, increases when the O_2 fraction decreases from 21% to 13%. Also the residence time in the soot area near CA50 increases during this part of the EGR-sweep. In combination, these trends are consistent with greater net soot production with decreasing O_2. It is reasonable to assume that the increased net soot production is partially associated with reduced soot oxidation at low O_2 fractions, although this cannot be quantified from the present data. Below 12% O_2, past the peak in smoke emissions, both the area growth rate and the residence time decrease. This should decrease the total net soot formation.

Experiments were performed together with Johan Sjöholm, Rikard Wellander, and Clemént Chartier. I post-processed the data and took the main responsibility of the paper writing which was carried out together with Johan Sjöholm, Rikard Wellander, and Öivind Andersson. The authors from the Division of Combustion Engines were the main responsible for the engine while the authors from the Division of Combustion Physics were the main responsible for the laser techniques.

7.5 Paper V

Impact of Mechanical Deformation due to Pressure, Mass, and Thermal Forces on the In-Cylinder Volume Trace In Optical Engines of Bowditch Design

Ulf Aronsson, Hadeel Solaka, Clément Chartier, Öivind Andersson, Bengt Johansson

Division of Combustion Engines, Lund University, Sweden

SIAT paper number 119 /SAE Technical paper 2011-26-008

This paper presents a detailed investigation of the impact of mechanical deformation on the in-cylinder volume as function of crank angle degree in an optical engine of Bowditch design. The squish height was found to change linearly with mass and pressure forces. It increases due to pressure forces and decreases due to mass forces. The thermal forces have an impact on the squish height but it is not clear in what direction. The volume change caused by deformations did not change the calculated load significantly but gave errors during heat release calculations. Two different strategies to reduce these errors are presented.

Experiments were carried out together with Hadeel Solaka and Clément Chartier. I post-processed the data and wrote the paper.

7.6 Paper VI

Analysis of Errors in Heat Release Calculations due to Distortion of the In-Cylinder Volume Trace from Mechanical Deformation for Optical Diesel Engines

Ulf Aronsson, Hadeel Solaka, Guillaume Lequien, Öivind Andersson, Bengt Johansson

[1]*Division of Combustion Engines, Lund University, Sweden*

Submitted to International Journal of Engine Research

Optical engines of Bowditch design may suffer from distortion of the in-cylinder volume trace due to mechanical deformation from mass, pressure and thermal forces. Errors in heat release calculation associated with such deformation were investigated in detail. The deformations were quantified by measuring the squish height during operation using high speed video. Deformations of all-metal engines were also estimated for comparison. The volume change caused by deformations caused errors in the heat release calculations both for optical and all metal engines. The errors at a given operating condition are smaller for all-metal engines but the importance is not necessarily smaller, since these engines normally are operated at higher loads. The errors can be eliminated by a corrected in-cylinder volume equation and motored heat release subtraction.

Experiments were carried out together with Hadeel Solaka and Guillaume Lequien. I post-processed the data and wrote the paper.

7.7 Paper VII

UHC and CO Emissions Sources from a Light-Duty Diesel Engine Undergoing Dilution Controlled Low-Temperature Combustion

Isaac W. Ekoto[1], Will F. Colban[1], Paul C. Miles[1,3]
Sung Wook Park[2], David E. Foster[2], Rolf D. Reitz[2]
Ulf Aronsson[3], Öivind Andersson[3]

[1]*Sandia National Laboratories*
[2]*University of Wisconsin Engine Research Center*
[3]*Division of Combustion Engines, Lund University, Sweden*

SAE Int. J. Engines March 2010 2:411-430/2009-24-0043

Sources of CO and UHC emissions were examined in an light-duty diesel engine during low load, early injection, and highly diluted conditions. The impact of engine load and charge dilution was also evaluated. The distribution of CO and UHC in the clearance volume were studied with spectrally resolved deep UV LIF with excitation near 230.1 nm. In addition results from PLIF at 355 nm, particle

image velocimetry (PIV), homogeneous reactor simulation, and multi dimensional simulation were utilized to analyze temperature fields, fluid flows and sources of CO and UHC in greater detail. Homogeneous reactor simulations showed that increased dilution leads to a narrower equivalence ratio (Φ) range that allows for acceptable UHC and CO oxidation. The cylinder center region contained intense near-injector fluorescence indicative of late-cycle fuel addition, while diffuse fluorescence was present from UHC and CO that was embedded in the surrounding fuel-lean bulk gases. Squish volume UHC and CO principally resulted from the partial oxidation of lean mixture, although UHC from piston top fuel films and crevice flows was also observed.

The first author, Isaac Ekoto, together with Paul Miles took the main responsibility for both the experiments and the paper writing. My part was connected to the deep UV LIF technique, to which I contributed the experimental setup and wrote parts of the evaluation code. I also assisted in the paper writing.

7.8 Paper VIII

UHC and CO Emissions Sources from a Light-Duty Diesel Engine Undergoing Late-Injection Low Temperature Combustion

Isaac W. Ekoto[1], Will F. Colban[1], Paul C. Miles[1,2]
Ulf Aronsson[2], Öivind Andersson[2]
Sung Wook Park[3], David E. Foster[3], Rolf D. Reitz[3]

[1]*Sandia National Laboratories*
[2]*Division of Combustion Engines, Lund University, Sweden*
[3]*University of Wisconsin Engine Research Center*

Proceedings of the ASME Internal Combustion Engine Division Fall Technical Conference ICEF September 27-30, 2009, Lucerne, Switzerland

Sources of CO and UHC emissions were examined in a light-duty diesel engine employing a late injection, low-temperature combustion strategy. The distribution of CO and UHC in the clearance volume were studied with spectrally resolved deep UV LIF with excitation near 230.1 nm. In addition results from PLIF at 355 nm, particle image velocimetry (PIV), homogeneous reactor simulation, and multi dimensional simulation were utilized to analyze temperature fields, fluid flows and sources of CO and UHC in greater detail. The measured spatial distributions show that fuel accumulated on the bowl-pip during high-temperature heat release was transported into the squish-volume by the reverse squish flow. Lean squish-volume mixtures, coupled with wall heat losses, severely inhibited squish volume fuel oxidation. Further retarding injection timing resulted in a two-fold increase in UHC emissions and a 33% increase in CO, primarily from the squish-volume.

The first author, Isaac Ekoto, together with Paul Miles took the main responsibility for both the experiments and the paper writing. My part was connected to the deep UV LIF technique, to which I contributed the experimental setup and wrote parts of the evaluation code. I also assisted in the paper writing.